N 62 14064
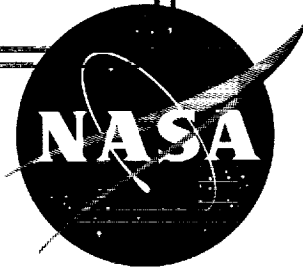
NASA TN D-1280

# TECHNICAL NOTE

## D-1280

APPROXIMATE ANALYSIS OF G LOADS AND HEATING DURING

ATMOSPHERIC ENTRIES AND PASSES WITH CONSTANT

AERODYNAMIC COEFFICIENTS

By Roger W. Luidens

Lewis Research Center
Cleveland, Ohio

NATIONAL AERONAUTICS AND SPACE ADMINISTRATION

WASHINGTON                                    July 1962

NATIONAL AERONAUTICS AND SPACE ADMINISTRATION

TECHNICAL NOTE D-1280

APPROXIMATE ANALYSIS OF G LOADS AND HEATING DURING

ATMOSPHERIC ENTRIES AND PASSES WITH CONSTANT

AERODYNAMIC COEFFICIENTS

By Roger W. Luidens

SUMMARY

Atmospheric braking offers significant reduction in vehicle size for space missions. An important phase of braking is the initial atmospheric entry. The present analysis yields approximate closed-form solutions applicable to atmospheric entries or passes of lifting or nonlifting vehicles with constant aerodynamic coefficients when the curvature of the flight path is less than the curvature of the planet surface. The variation of atmospheric density, G load, and heating rate with distance along the flight path and peak values of G load and heating rate are determined. The total heat input is given as a function of the velocity decrease and G load.

The flight paths exhibit a characteristic variation of atmospheric density as a function of distance along the path, which has the form of the Gaussian error curve. For entries or passes with a small velocity decrease, peak values of G load and heating rate occur approximately at the minimum-altitude point; however, for flights with appreciable velocity decreases, the peak values occur prior to this point.

An analysis of several atmospheric entries followed by deceleration to zero velocity showed that the maximum heat input to the vehicle windward side occurred on the undershoot bound, and the maximum leading-edge heating on the overshoot bound. The vehicle-design heat load is a combination of the aforementioned maximums and is greater than the heat load on a single flight path.

INTRODUCTION

Deceleration by atmospheric drag, in lieu of decelerating rockets, offers the possibility of a significant reduction in the size of vehicles required for space missions (e.g., ref. 1). In order to evaluate the

applicability of atmospheric braking, the flight trajectories of entry
vehicles must be studied, because the associated heating and deceleration
loads determine the weights required for structure and heat-protection
systems.

Two general categories of atmospheric-braking trajectories are pos-
sible. In the first, a series of "passes" is made through the atmosphere
in which a comparatively small amount of deceleration is accomplished
during each single pass. (Of course, the first pass must reduce the ve-
hicle's velocity to less than the escape value.) The entry altitude and
the magnitude of the deceleration determine whether the pass may be ac-
complished using either positive or negative lift, or none at all
(figs. l(a), (b), and (c)).

In the second general category of atmospheric-braking trajectories,
the vehicle is not permitted to leave the atmosphere after having entered,
and the full deceleration is accomplished in a continuous maneuver. For
purposes of analysis, it is convenient to consider this maneuver in three
separate phases (fig. l(d)): the initial "entry" phase (which is iden-
tical with an atmospheric pass up to the point of minimum altitude), a
short, intermediate "transition" phase, and, finally, a "deceleration"
phase. Although the velocity reduction that occurs during the entry
phase is important, the entry phase is of particular interest, because
this portion of the flight determines the depth of the entry corridor,
the boundaries of which are shown in figure l(e).

The most accurate method of calculating the deceleration and heating
during atmospheric braking is numerical integration of the differential
equations of motion and heat transfer (e.g., refs. 2 and 3); however, ap-
proximate closed-form solutions may offer the advantages of simplicity
of calculation, exhibition of significant parameters, and clarification
of the interrelation between variables.

For vehicles having zero lift, references 4 and 5 offer closed-form
solutions for the ballistic parameter $W/C_DA$, fixed and modulated. (All
symbols are defined in appendix A.) For vehicles with lift, reference 6
gives solutions for the deceleration phase for vehicles using modulated
$W/C_LA$. Reference 7 gives solutions for corridor depths and maneuver
loads for the entry phase (with both constant and variable aerodynamic
coefficients). The analysis presented herein extends reference 7 to con-
sider the heating during the entry phase and also considers the decelera-
tion and heating during atmospheric passes. Both lifting and nonlifting
flight is included, but the study is restricted to the use of constant
aerodynamic coefficients.

Approximate closed-form expressions are obtained for the variation
of heating rate, maneuver load, and atmospheric density along the flight

path. Peak values of these quantities and the total heat input are also obtained. The accuracy and the method of application of the results are illustrated.

## ANALYSIS

The velocity change, laminar convective heating, and G load during an atmospheric entry or an atmospheric pass are analyzed for vehicles operating with constant aerodynamic coefficients (i.e., $C_L$, $C_D$, $C_R$, and W constant). The phase of the atmospheric flight termed entry begins at the "edge" of the atmosphere, station 0 (fig. 2) and ends at the position along the flight path where the altitude is a minimum, station 2. (For the pass or entry, station 2 is the point of maximum density and zero path angle with respect to the local horizontal as well as the minimum-altitude point. Of course, lower altitudes can occur on phases of the flight path subsequent to the entry.) A pass includes the continuation of such a flight path until it exits from the atmosphere, station 4.

### Initial Relations and Assumptions

Equations of motion. - The following initial assumptions are made as is usual for simple analyses: (1) The planet and the atmosphere are spherically symmetric, (2) the rotation of the planet and atmosphere is neglected, (3) the motion occurs in a plane, and (4) the range of altitudes h where the aerodynamic forces are significant is very small compared with the planet radius r, so that $\sqrt{gr}$ may be taken as a constant. In an inertial reference system, the equations of motion tangent and normal to the flight path may be written in terms of the nomenclature of figure 2 as

$$- \frac{1}{g} \frac{dV}{d\tau} = \frac{C_D \rho V^2 A}{2W} + \sin \varphi \tag{1}$$

$$- \frac{V}{g} \frac{d\Omega}{d\tau} = \frac{C_L \rho V^2 A}{2W} - \cos \varphi \tag{2}$$

The first equation is simplified by assuming that $\sin \varphi$ is small compared with the dimensionless aerodynamic force and, hence, can be neglected. In the second equation, it is assumed that $\varphi$ is small enough that $\cos \varphi$ is approximately 1. The validity of these assumptions is discussed in appendix B.

4

A rectangular coordinate system $x,y$ is defined with the origin at the minimum-altitude point of the flight path (station 2) and with the positive y-axis directed through the center of the earth (fig. 2). With respect to this coordinate system, the flight-path angle with reference to the x-direction $\gamma$ is always assumed small while the vehicle is significantly influenced by the atmosphere; therefore,

$$dx = ds \cos \gamma \approx ds \qquad (3)$$

With the assumption that $\varphi - \gamma$ is small also,

$$h \approx (y_e - y_f)\cos(\varphi - \gamma) \approx y_e - y_f \qquad (4)$$

($y_f$ is negative as shown in fig. 2). The following relations are then used in equations (1) and (2), respectively,

$$\frac{dV}{dx} \approx \frac{dV}{ds} = \frac{dV}{d\tau}\frac{1}{\frac{ds}{d\tau}} = \frac{1}{V}\frac{dV}{d\tau} \qquad (5)$$

$$\frac{d\Omega}{d\tau} = \frac{V}{r_{f,i}} \qquad (6)$$

to obtain

$$-\frac{dV}{V} = \frac{gC_D A\rho \; dx}{2W} \qquad (7)$$

and

$$r_{f,i} = \frac{V^2}{g\left(1 - \dfrac{C_L\rho V^2 A}{2W}\right)} = \frac{V^2}{g - \dfrac{C_L\rho V^2 A}{2m}} \qquad (8)$$

Representation of atmosphere. - The density variation of the atmosphere with altitude is assumed to be exponential:

$$\rho = \rho_{h=0}e^{-\beta h} \qquad (9)$$

where, for earth, the values $\beta^{-1} = 2.35\times10^4$ feet and $\rho_{h=0} = 0.0027$ slug per cubic foot yield a good "fit" to the atmosphere at entry altitudes (ref. 2). From equation (9)

$$\frac{d\rho}{dh} = -\beta\rho \qquad (10)$$

Heating relations. - If a laminar boundary layer is assumed, the heating rate in Btu per square foot per second may be written, according to reference 6, as

$$\dot{q} = j\rho^{1/2}V^3 \tag{11}$$

where, for a two-dimensional leading edge (eq. (9), ref. 6),

$$j_l \equiv \frac{15.5 \times 10^{-9} \cos \lambda \cos^\nu \Lambda_{ef}}{R_N^{1/2}} \tag{12}$$

and for the windward side of the vehicle (eq. (C15), or combination of (C16) and (C18), ref. 6)

$$j_W \equiv 15.75 \times 10^{-9} \sqrt{\frac{\cos \alpha \sin^2\alpha}{\xi}} \tag{13}$$

The G load is defined by

$$G = \frac{C_R \rho V^2 A}{2W} \tag{14}$$

so that $\dot{q}$ (eq. (11)) may be written

$$\dot{q} = j \sqrt{\frac{2WG}{C_R A}} V^2 \tag{15}$$

Finally, the preceding equations are written in the forms used subsequently:

$$\frac{\dot{q}_l}{\sqrt{\frac{W}{AR_N}} \cos^\nu \Lambda_{ef} \cos \lambda} = 15.5 \times 10^{-9} \sqrt{\frac{2G}{C_R}} V^2 \tag{16}$$

$$\frac{\dot{q}_W}{\sqrt{\frac{W}{A\xi}}} = 15.75 \times 10^{-9} \sqrt{\frac{2G \cos \alpha \sin^2\alpha}{C_R}} V^2 \tag{17}$$

The heat input per square foot $q$ may be written in the following form, where $V = ds/d\tau \approx dx/d\tau$

$$q \equiv \int_{\tau_i}^{\tau_f} \dot{q} \, d\tau = \int_{x_i}^{x_f} \frac{\dot{q} \, dx}{V} \qquad (18)$$

The total heat input $Q$ is obtained by integrating the heat input per square foot over the leading-edge region and the windward side of the vehicle:

$$Q = \int_{A_l} q_l \, dA_l + \int_{A_w} q_w \, dA_w \qquad (19)$$

The heat input to lee and base regions is assumed small compared with the aforementioned heat inputs and, hence, can be neglected.

### Density Variation Along Flight Path

Integration of equation (7) to obtain the velocity change requires a relation between $\rho$ and $x$. This relation is obtained by assuming that the flight path and the surface of the planet can each be represented by a single segment of a parabola with the axis of symmetry on the y-axis of the x,y-coordinate system of figure 2. (For greater accuracy, the representation of the flight path by a power series may be considered. The present parabolic assumption is equivalent to consideration of the first several terms of such a series. The ultimate justification for this approach lies in the accuracy of the results achieved.) The equations for the flight path and the surface of the planet are, respectively,

$$y_f = \frac{x^2}{2r_f} \qquad (20)$$

$$y_e = h_2 + \frac{x^2}{2r} \qquad (21)$$

where $r_f$ and $r$ are the radii of curvature at the vertices of the parabolas. For the surface of the planet, $r$ is the radius of the planet. The selection of $r_f$ is discussed in appendix B. As the flight path is drawn in figure 2, $r_f$ is negative in the vicinity of station 2. With

the assumptions of equations (3) and (4), the altitude of the flight path above the planet surface is

$$h = y_e - y_f = h_2 + \frac{x^2}{2}\left(\frac{1}{r} - \frac{1}{r_f}\right) \tag{22}$$

and

$$\frac{dh}{dx} = x\left(\frac{1}{r} - \frac{1}{r_f}\right) \tag{23}$$

Then from the mathematical identity

$$\frac{d\rho}{dx} = \frac{d\rho}{dh}\frac{dh}{dx} \tag{24}$$

equations (10) and (23) may be combined to yield

$$\frac{d\rho}{\rho} = -ax \, dx \tag{25}$$

where

$$a \equiv \beta\left(\frac{1}{r} - \frac{1}{r_f}\right) \tag{26}$$

From the previous assumptions, $a$ is a constant, and equation (25) may be integrated from $x = 0$ (where $\rho = \rho_2$) to the general position $x$ to give

$$\frac{\rho}{\rho_2} = e^{-ax^2/2} \tag{27}$$

Equation (27) has the form of the Gaussian error curve. The variation of the density ratio $\rho/\rho_2$ with the distance parameter $p = x\sqrt{a/2}$ is shown in figure 3. (The variation is independent of flight-path parameter $F$, which distinguishes the three parts of fig. 3.) The initial entry into the atmosphere occurs at a negative value for $x$ and, hence, at a negative $p$.

## Velocity Variation Along Flight Path

The velocity variation about the minimum-altitude point, station 2, may be obtained by integrating equation (7) between station 2, where $x = 0$, and the general point $x$. If a constant drag coefficient $C_D$ is assumed and the result for the atmospheric density variation given by equation (27) is used, equation (7) becomes

$$-\int_{V_2}^{V} \frac{dV}{V} = \frac{gC_D A\rho_2}{2W} \int_0^x e^{-ax^2/2}\, dx \tag{28}$$

The integral on the right may be transformed into the standard form of the error function by the substitution of

$$p = \sqrt{\frac{a}{2}}\, x; \qquad dp = \sqrt{\frac{a}{2}}\, dx \tag{29}$$

so that equation (28) may be written as

$$\ln \frac{V}{V_2} = \frac{-gC_D A\rho_2}{4W} \sqrt{\frac{2\pi}{a}} \left( \frac{2}{\sqrt{\pi}} \int_0^{p(x)} e^{-p^2}\, dp \right) \tag{30}$$

The upper limit required to evaluate the integral may also be written as

$$p(x) = \sqrt{\frac{a}{2}}\, x = \pm\sqrt{-\ln \frac{\rho}{\rho_2}} \tag{31}$$

by using equation (27). The value of the term in parentheses required in equation (30) is tabulated in reference 8 as a function of $p(x)$ and is designated $P(p)$ herein. From the definition of $G$ given by equation (14), the result may be written as

$$\frac{V}{V_2} = e^{FP(p)} \tag{32}$$

The coefficient $F$ of $P(p)$ is a constant for a given flight path defined as

$$F \equiv \frac{C_D G_2 g}{C_R V_2^2} \sqrt{\frac{\pi}{2\beta\left(\dfrac{1}{r} - \dfrac{1}{r_f}\right)}} \tag{33}$$

where $r_f$ is given by equation (B6). The parameter F is referred to as the flight-path parameter. It includes the effects of the vehicle aerodynamic characteristics $C_D$, $C_R$, and $C_L$, where $C_L$ occurs in $r_f$; the planetary and atmospheric characteristics g, r, and β; and the flight-path characteristics G load and velocity at station 2. Typical variations of the velocity ratio $V/V_2$ with the distance parameter p are shown in figure 3.

Specification of the conditions at station 2, namely $V_2$, $G_2$, $C_D/C_R$, and $C_L/C_R$ in the preceding relations, corresponds to entering the earth's atmosphere from space at some particular entry velocity. This velocity may be determined by choosing an upper limit in equation (30) corresponding to an x of large magnitude. When x (or $x_0$) becomes large, a number of the original assumptions, for example, φ and γ small and the parabolic approximation, become poor; however, concurrently, the influence of the atmosphere on the path falls markedly because of the rapid diminution of the density with x (e.g., the variation of the density ratio $\rho/\rho_2$ with the distance parameter $p \equiv \sqrt{a/2}\, x$, fig. 3). The desired integral from equation (30) may be written as

$$-\int_0^{p(x_0)} e^{-p^2}\, dp = \int_0^{-p(x_0)} e^{-p^2}\, dp = \int_0^{\infty} e^{-p^2}\, dp - \int_{-p(x_0)}^{\infty} e^{-p^2}\, dp$$

(34)

where the last term encompases only the region of large x. It is shown in appendix B that the last term is, in general, of negligible magnitude compared with the preceding term, which is the standard form of the error function. Thus, errors in the last term, because of an inaccurate description of the flight path, can have little effect on the value of the original integral. The value for the integral that occurs in equation (30) may, therefore, be taken as the value of the standard form. For entry from space, then,

$$P(p) = \frac{2}{\sqrt{\pi}} \int_0^{\infty} e^{-p^2}\, dp = 1.0$$

(35)

and equation (32) becomes

$$\frac{V_0}{V_2} = e^F \tag{36}$$

Similarly, for the exit phase of a pass through the atmosphere,

$$\frac{V_4}{V_2} = e^{-F} \tag{37a}$$

The combination of equations (36) and (37a), then yields the entrance-to exit-velocity ratio for an atmospheric pass,

$$\frac{V_0}{V_4} = e^{2F} \tag{37b}$$

The manner in which the initial- to final-velocity ratios during an atmospheric entry $V_0/V_2$ and during an atmospheric pass $V_0/V_4$ vary with the flight-path parameter $F$ is shown in figure 4. These curves may be used to interrelate the velocity ratios to the parameter $F$, which is used as an independent variable for several subsequent calculations.

With the variation of the atmospheric density and the velocity along the flight path determined, the variation of the G load and heating rate may be readily calculated.

### G Load Variation Along Flight Path

The variation of G load along the flight path can be conveniently described by forming the ratio of the G load at any location to its value at station 2. From equation (14)

$$\frac{G}{G_2} = \frac{\rho}{\rho_2}\left(\frac{V}{V_2}\right)^2 \tag{38}$$

The ratio $G/G_2$ as a function of the distance parameter $p$ can be evaluated by using equations (31) and (32), which relate $\rho/\rho_2$ and $V/V_2$ to $p$ for a given value of $F$; typical results are shown in figure 3. From such plots, the maximum values $G_{max}/G_2$ can be ascertained. In figure 4, the ratio $G_{max}/G_2$ is plotted against $F$. In equations (32) and (33), the velocity variation is given in terms of $G_2$. Figure 4

gives the required relation between $G_2$ and $G_{max}$, which permits determination of the velocity variation in terms of $G_{max}$.

## Heating-Rate Variation Along Flight Path

The ratio of the heating rate along the flight path to the heating rate at station 2 is, from equation (11),

$$\frac{\dot{q}}{\dot{q}_2} = \left(\frac{\rho}{\rho_2}\right)^{1/2} \left(\frac{V}{V_2}\right)^3 \tag{39}$$

This ratio may be evaluated in the same manner as the $G$ ratio; typical results are shown in figure 3. The peaks of these curves $\dot{q}_{max}/\dot{q}_2$ are also plotted in figure 4 as functions of $F$.

## Heat Input Per Unit Area

From equations (18), (27), and (39), the total heat input per unit area during the entry phase (from station 0 to station 2) may be written as

$$q_{0,2} = \frac{\dot{q}_2}{V_2} \int_{x_0=-\infty}^{x_2=0} \left(\frac{V}{V_2}\right)^2 e^{-ax^2/4} \, dx \tag{40}$$

The term $V/V_2$ as a function of $x$ is given by equation (32), but this form is not readily dealt with. Hence, a straight-line approximation to the velocity variation, illustrated in figure 5 and defined by the following equations, is used:

$$\frac{V}{V_2} = 1 + \frac{1}{V_2}\left(\frac{dV}{dx}\right)_2 x \qquad \text{for} \quad x_a \leq x \leq 0$$

and

$$\frac{V}{V_0} = 1 \qquad \text{for} \quad x \leq x_a \tag{41}$$

where using equations (7), (14), and (33) gives

$$\left(\frac{dV}{dx}\right)_2 = \left(\frac{dV}{d\tau}\right)_2 \frac{1}{\left(\frac{dx}{d\tau}\right)_2} = \frac{-G_2 g}{V_2}\frac{C_D}{C_R} = \frac{-BV_2}{2}\sqrt{\frac{a}{2}} \qquad (42a)$$

where

$$B \equiv \frac{2C_D G_2 g}{C_R V_2^2}\sqrt{\frac{2}{a}} \qquad\qquad \text{(Note: } B = \frac{4}{\sqrt{\pi}}\,F\text{)}$$

and

$$x_a \equiv \frac{V_0 - V_2}{\left(\frac{dV}{dx}\right)_2} \qquad (42b)$$

The comparison in figure 5 shows that the approximate velocity variation is a good representation of the actual velocity variation. With the use of the approximate velocity variation, equation (40) becomes

$$q_{0,2} = \frac{\dot{q}_2}{V_2}\left[\int_{x_a}^{0} e^{-ax^2/4}\,dx - \frac{2G_2 g C_D}{V_2^2 C_R}\int_{x_a}^{0} x e^{-ax^2/4}\,dx\right.$$

$$\left. + \left(\frac{G_2 g C_D}{V_2^2 C_R}\right)^2\int_{x_a}^{0} x^2 e^{-ax^2/4}\,dx + \left(\frac{V_0}{V_2}\right)^2\int_{x=-\infty}^{x_a} e^{-ax^2/4}\,dx\right] \qquad (43)$$

Writing this equation in terms of $B$ and $p$ yields

$$q_{0,2} = \frac{\dot{q}_2}{V_2}\sqrt{\frac{2}{a}}\left[\int_{p_a}^{0} e^{-p^2/2}\,dp - B\int_{p_a}^{0} p e^{-p^2/2}\,dp\right.$$

$$\left. + \frac{B^2}{4}\int_{p_a}^{0} p^2 e^{-p^2/2}\,dp + \left(\frac{V_0}{V_2}\right)^2\int_{p=-\infty}^{p_a} e^{-p^2/2}\,dp\right] \qquad (44)$$

In accordance with an argument similar to that following equation (31), the lower limit of the last integral has been replaced by negative infinity. The integrals may be evaluated in terms of known quantities. The result for the heat input per square foot during an atmospheric entry is

$$q_{0,2} = \frac{\dot{q}_2}{V_2} \sqrt{\frac{2}{a}} \, N_{0,2} \tag{45a}$$

where

$$N_{0,2} \equiv \sqrt{\frac{\pi}{2}} \, P\left(\left|\frac{p_a}{\sqrt{2}}\right|\right) + B\left(1 - e^{-p_a^2/2}\right)$$

$$+ \frac{B^2}{4}\left[p_a e^{-p_a^2/2} + \sqrt{\frac{\pi}{2}} \, P\left(\left|\frac{p_a}{\sqrt{2}}\right|\right)\right] + \left(\frac{V_0}{V_2}\right)^2 \sqrt{\frac{\pi}{2}}\left[1 - P\left(\left|\frac{p_a}{\sqrt{2}}\right|\right)\right] \tag{45b}$$

$p_a$ is determined by equations (31) and (42b), and $V_0/V_2$ by equation (36). Ultimately, $N_{0,2}$ depends only on $F$.

A similar analysis of the heat input subsequent to station 2 yields

$$q_{2,4} = \frac{\dot{q}_2}{V_2} \sqrt{\frac{2}{a}} \, N_{2,4} \tag{46a}$$

where

$$N_{2,4} \equiv \sqrt{\frac{\pi}{2}} \, P\left(\frac{p_b}{\sqrt{2}}\right) - B\left(1 - e^{-p_b^2/2}\right)$$

$$+ \frac{B^2}{4}\left[- p_b e^{-p_b^2/2} + \sqrt{\frac{\pi}{2}} \, P\left(\frac{p_b}{\sqrt{2}}\right)\right] + \left(\frac{V_4}{V_2}\right)^2 \sqrt{\frac{\pi}{2}}\left[1 - P\left(\frac{p_b}{\sqrt{2}}\right)\right] \tag{46b}$$

and $p_b$ is the value of $p$ at

$$x_b \equiv \frac{V_4 - V_2}{\left(\frac{dV}{dx}\right)_2} \tag{46c}$$

The heat input for an atmospheric pass is given by the sum of equations (45) and (46):

$$q_{0,4} = \frac{\dot{q}_2}{V_2} \sqrt{\frac{2}{a}} \, N_{0,4} \tag{47a}$$

where

$$N_{0,4} = N_{0,2} + N_{2,4} \tag{47b}$$

Equations (45), (46), and (47) may be evaluated with aid of figure 6 in which are plotted the functions $N_{0,2}$, $N_{2,4}$, and $N_{0,4}$ as functions of F. Note that the deviation of $N_{0,4}$ from the constant value of $\sqrt{2\pi}$ is small for small values of F.

In some instances, it may be desirable to write the relation for the heat input for an atmospheric entry (eq. (45)) or pass (eq. (47)) explicitly in terms of the initial and final velocities. An example of such a relation is given in appendix C.

### Total Heat Input

The value of total heat input to a vehicle is found by integrating the heat input per square foot over the surface (eq. (19)). As an example, the integrations carried out in reference 6 for the configuration shown in figure 7 are given. The vehicle is a delta-wing configuration and the useful volume is assumed to be the volume of the wing. The vehicle is characterized by gross weight W, fuselage density $\rho_f$, sweepback angle $\Lambda$, and wing loading W/A. These parameters define the vehicle geometry and aerodynamics including $(L/D)_{max}$. The result of the integration over the leading edge is (ref. 6, table I, col. 17 where $\cos \Lambda_{ef} = (1 - \sin^2\Lambda \cos^2\alpha)^{1/2}$)

$$\frac{Q_l}{W} = \frac{q_l}{\sqrt{\frac{W}{R_N A}} \cos^\nu\Lambda_{ef} \cos\lambda} \frac{\sqrt{2} \, k_l \cos^{\nu-1}\Lambda}{\left(\frac{\rho_f W \tan\Lambda}{W/A}\right)^{1/2}} \tag{48}$$

and over the windward side is (ref. 6, table I, col. 18)

$$\frac{Q_w}{W} = \frac{q_w}{\sqrt{\frac{W}{A\xi}}} \frac{8}{3} \frac{k_w}{\left(W \frac{W}{A} \tan\Lambda\right)^{1/4}} \tag{49}$$

The  k  terms are constants that depend on the vehicle geometry and are discussed in appendix D. The terms $q_l$ and $q_w$ are determined by combining equations (16) or (17) with equations (46) or (47).

## Flight Time

An estimation of the flight time may be made by using the approximation to the velocity variation given by equation (41). For example, in the region from  $x = 0$  to  $x_a$  of the entry phase of the flight, the elapsed time measured from station 2 (which is negative) is

$$\int_{\tau_2}^{\tau_x} d\tau = \int_{x=0}^{x} \frac{dx}{V_2 + \left(\frac{dV}{dx}\right)_2 x} \tag{50}$$

which yields, by using equation (42),

$$-\tau_{2,x} = \frac{V_2 C_R}{G_2 g C_D} \ln\left(1 - \frac{G_2 g C_D}{V_2^2 C_R} x\right) \tag{51}$$

## Sample Calculation Procedure

A typical entry problem may be stated as: Given the entry velocity $\overline{V}_0$ and maximum G load  $G_{max}$, find the velocity at the end of the entry phase (station 2), the maximum heating rate  $\dot{q}_{max}$, and the total heat input  $Q/W$  during the entry phase of the flight. The developments of the preceding paragraphs give results in terms of conditions at station 2 (i.e., $\overline{V}_2$ and  $G_2$), which in the previously stated problem are unknown quantities. Hence the conditions at station 2 must be determined first. From equations (26), (33), (36), and (B6),

$$\overline{V}_2 = \overline{V}_0 e^{-F} \tag{52a}$$

where

$$F = \sqrt{\frac{\pi}{2\beta r}} \frac{C_D}{C_R} \frac{G_2}{\overline{V}_2^2} \sqrt{1 - \frac{1 - 0.85 \, G_2 \left(\frac{C_L}{C_R}\right)}{\overline{V}_2^2}} \qquad (52b)$$

The G load at station 2 may be written as

$$G_2 = \frac{G_{max}}{\left(\dfrac{G_{max}}{G_2}\right)} \qquad (53)$$

where the term in parentheses is a function of $F$ and is shown in figure 4. An iteration procedure is used to find the solution to the preceding relations. For an example, consider the entry into the Earth's atmosphere ($\sqrt{\beta r}$ = 30, see ref. 2) at $\overline{V}_0$ = 2.0, at zero lift (i.e., $C_L/C_R$ = 0; $C_D/C_R$ = 1.0) with $G_{max}$ = 10. The results of four iterations are shown in the following table:

| Param-<br>eter | Iteration | | | |
|---|---|---|---|---|
| | 1 | 2 | 3 | 4 |
| $F$ | 0.1207 | 0.159 | 0.174 | 0.180 |
| $G_2$ | 9.9 | 9.81 | 9.75 | 9.70 |
| $\overline{V}_2$ | 1.775 | 1.705 | 1.68 | 1.67 |

The first approximation is obtained by letting $G_2 = G_{max} = 10$ and $\overline{V}_2 = \overline{V}_0 = 2.0$. The flight-path parameter $F$ may then be calculated, from which better estimates of $G_2$ and $\overline{V}_2$ are obtained. The precision of the fourth iteration is probably within the accuracy of the method of analysis.

The parameters $\overline{V}_2$ and $G_2$ having been determined, the peak heating rate may be obtained from the relation

$$\dot{q}_{max} = \dot{q}_2 \left( \frac{\dot{q}_{max}}{\dot{q}_2} \right)$$

where $\dot{q}_2$ is determined by equation (16) or (17) evaluated at station 2, and the term in parentheses is a function of $F$ given in figure 4. The total heat input is given by equation (45a), which is in terms of conditions at station 2, in combination with equations (48) and (49). Numerical results of several of the preceding calculations are given in table I.

For generalized results that apply to atmospheric passes, explicit solutions, outlined in appendix C, are possible.

## DISCUSSION

Many assumptions, the validity of which is determined ultimately by the accuracy achieved, have been made. Therefore, the results of the present analysis are first compared with results of more accurate published solutions, and then some typical applications are shown.

### Comparison of Present Analysis with Other Calculations

Reference 2 contains the results of a study of atmospheric passes with constant aerodynamic coefficients, which were obtained by numerical integration on a digital computing machine. A comparison is made with results obtained by the method of the present report in figure 8. For a constant entry velocity, the effects of vehicle lift-drag ratio and dimensionless exit velocity $\overline{V}_4$ on the G load and the heating are shown. (The procedure for reducing the present results to the form of ref. 2 is described in appendix C.)

For the most part, the present analysis adequately determines the relation of velocity change to peak G load, peak heating rate, and stagnation point heat input per square foot. The largest errors occur where the exit velocity $\overline{V}_4$ is near unity and where lift is negative. At these conditions, the curvature of the flight path approaches the surface curvature of the planet. Reduced accuracy results because the parameter $a$ (eq. (26)) approaches zero and $F$ (eq. (33)), used in equations (36) and (37), approaches infinity. In general, if the flight path curvature does not approach the planet surface curvature, the present solutions will be adequate for preliminary analyses.

## Variation of Entry Parameters Along Flight Path

The variation of velocity, atmospheric density, G load, and heating rate with distance along a typical atmospheric pass (or entry) is shown in figure 3. Maximum values of the entry parameters occur in the following order in terms of distance or time from the initial "edge" of the atmosphere: heating rate, G load, and density. For larger values of F, peak values of G load and heating rate can be significantly above the values at the point of minimum altitude and occur prior to that point. A comparison of the curves of the three parts of figure 3 shows that for small values of F, which occur for small velocity changes, peak values of heating rate and G load occur approximately at the minimum-altitude point.

## Sample Application

As an example of the application of the present analysis, the heating loads with a constraint on the G load are analyzed for the entry and deceleration segments of several flight paths similar to those of figure 1(d) and (e). The present analysis yields the heating and G loads during the entry; reference 7 gives the corridor depth as a function of the G load, and reference 6 gives the deceleration flight-path characteristics. The entry vehicle analyzed (fig. 7) has a maximum lift-drag ratio of 1 and a gross weight of 10,000 pounds. Further detailed numerical values are given in appendix D.

It is assumed that the vehicle is protected from aerodynamic heating by an ablating surface material. An important criterion of the merit of such a heat-protection system is the ablated weight as a fraction of the vehicle gross weight $W_p/W$. If the ablating material has an effective heat of ablation $C$, which is independent of velocity, the heat-protection weight is related to the heat input per pound of vehicle gross weight $Q/W$ by the expression $W_p/W = C^{-1}(Q/W)$. The present example considers the parameter $Q/W$.

Table I presents a comparison of the heat input along several different atmospheric-braking paths. In each case the initial velocity $\overline{V}_0$ is 2.0 and the terminal velocity is zero. In table I(a), the vehicle is

assumed to enter the atmosphere along the undershoot bound[1], and the entry is followed by a constant 10-G deceleration[2]. The velocity ratio $\bar{V}$ that divides the two segments of the flight path is 1.90, as shown in the sketch. Of the various entry paths considered, this case incurs the greatest heat input to the windward side.

In table I(b) the vehicle enters the atmosphere along the overshoot bound[3], and again the entry is followed by a 10-G deceleration phase. The altitude of the overshoot bound above the undershoot bound, shown in the last column of table I, is 10.5 miles; this altitude difference is the entry corridor depth. Braking along this type of bound yields a total heat input slightly less than that of the undershoot bound, although the leading-edge heating is greater.

For the flight path of table I(c), the entry phase ends very nearly tangent to the 10-G deceleration path. This entry occurs near the middle of the entry corridor (last column, table I). The total heat input along this path is less than along either of the two bounds. About one-half of the total heat input occurs during the entry phase, which indicates the importance of the ability to analyze this phase of the flight path.

If the greatest relaxation in the accuracy required of the planet approach guidance systems is to be permitted, it is necessary to design the entry vehicle to tolerate conditions encountered on the overshoot and

---

[1]"Undershoot bound" denotes the lowest acceptable flight path that the vehicle can follow. In this report, the bound is defined as the path that corresponds to a 10-G deceleration load at the end of the entry phase when the vehicle has held a constant 23° angle of attack during the entry. (The 23° limit is imposed to keep the heat input from hot-gas radiation small compared with the convective heat input.)

[2]In refs. 6 and 9 the constant-G type of deceleration flight path was found to give the lowest heat input for a given G limit.

[3]"Overshoot bound" is the highest acceptable entry path. It is defined here as the condition in which the vehicle has a 10-G maneuver capability at a 23° angle of attack at the end of the entry phase, point A. During the entry phase, however, the angle of attack is held at 0°, for which the G load at point A is 3.4. The 10-G capability is used to accomplish the transition maneuver between the entry and deceleration phases. Although this transition has not been studied, it is expected to increase the heating to the windward side somewhat with little effect on the leading-edge heating. An overshoot bound defined as the "highest altitude at which constant-angle-of-attack flight within the atmosphere can be maintained" can yield heat inputs 4.9 times greater than that obtained with the present definition (ref. 6, p. 22).

undershoot bounds and along any path within the entry corridor. Thus, the vehicle must be designed for the maximum windward-side heat input (i.e., that of the undershoot bound) and the maximum leading-edge heat input (i.e., that of the overshoot bound). The design heat input, the sum of these two maximums, is greater than the heat input on any single flight path, that is, 9 percent greater than the heat input along the undershoot bound.

## SUMMARY OF RESULTS

Approximate closed-form expressions were obtained for the variation along the flight path of atmospheric density, G load, and heating rate for the assumption of a laminar boundary layer. Also obtained were peak values of these quantities, heat input per square foot, and total heat input. These quantities are functions of the velocity change during an atmospheric entry or pass. The solutions are applicable to lifting and nonlifting vehicles with constant aerodynamic coefficients when the curvature of the flight path is less than that of the planet surface curvature. The more significant conclusions are:

1. These simple closed-form solutions can describe the aerodynamic and thermodynamic characteristics of atmospheric entries and passes with an accuracy adequate for preliminary analysis.

2. The flight paths exhibit a characteristic variation of the atmospheric density as a function of distance along the flight path, which has the form of the Gaussian curve of error.

3. A number of parametric groupings and interrelations have been determined. For example, the initial- to final-velocity ratio $V_0/V_4$ for an atmospheric pass is

$$\frac{V_0}{V_4} = e^{2F}$$

with

$$F = \frac{C_D}{C_R} \frac{G_2 g}{V_2^2} \sqrt{\frac{\pi}{2\beta\left(\frac{1}{r} - \frac{1}{r_f}\right)}}$$

where $C_D/C_R$ is the ratio of drag to resultant force, $G_2$ and $V_2$ are the G load and velocity at the minimum-altitude point, $\beta$ is the exponential decay rate of atmospheric density, $r$ and $r_f$ are the radius of

the planet and the flight path, respectively, and $g$ is gravitational acceleration.

4. For atmospheric entries and passes with a small velocity decrease, peak values of G load and heating rate occurred approximately at the minimum-altitude point; however, for flights with an appreciable velocity decrease, the peak values of G load and heating rate were significantly larger than the values at the point of minimum altitude and occurred prior to that point.

5. An analysis of several atmospheric entries followed by decelerations to zero velocity showed that the maximum heat input to the vehicle windward side occurred on the undershoot bound, and the maximum leading-edge heating on the overshoot bound. The vehicle-design heat load is a combination of the aforementioned maximums and is greater than the heat load on any single flight path.


Lewis Research Center
    National Aeronautics and Space Administration
        Cleveland, Ohio, March 23, 1962

## APPENDIX A

### SYMBOLS

A      reference area for aerodynamic coefficients; plan area of vehicle, sq ft

a      $\beta\left(\dfrac{1}{r} - \dfrac{1}{r_f}\right)$

B      $2\,\dfrac{C_D}{C_R}\,\dfrac{G_2 g}{V_2^2}\,\sqrt{\dfrac{2}{a}}$

b      span of vehicle (fig. 7)

$C_D$      aerodynamic drag coefficient, $\dfrac{D}{\frac{1}{2}\,\rho V^2 A}$

$C_L$      aerodynamic lift coefficient, $\dfrac{L}{\frac{1}{2}\,\rho V^2 A}$

$C_R$      aerodynamic resultant force coefficient, $\dfrac{\text{resultant force}}{\frac{1}{2}\,\rho V^2 A}$   or

$$C_R = \sqrt{C_L^2 + C_D^2}$$

c      root chord of vehicle, ft

D      drag

d      corridor depth, ft

d'      thickness of vehicle (fig. 7)

F      flight-path parameter, $\dfrac{C_D G_2 g}{C_R V_2^2}\,\sqrt{\dfrac{\pi}{2a}}$

f      linear distance along streamline from nose stagnation point to end of nose region, or beginning of windward side (see fig. 7)

| | |
|---|---|
| f | linear distance along streamline from nose stagnation point to end of nose region, or beginning of windward side (see fig. 7) |

$f/c$     $\dfrac{\pi}{4}\dfrac{R_N}{c}\left(1 + \dfrac{1}{\cos \Lambda} - \dfrac{4}{\pi}\arctan\dfrac{\tan \alpha}{\cos \Lambda}\right)$ (from appendix E, ref. 6)

| | |
|---|---|
| G | vehicle acceleration/g |
| g | acceleration due to gravity, essentially planet surface value, 32.2 ft/sec$^2$ for earth |
| h | altitude, ft |
| $h_p$ | vacuum perigee altitude of planet approach trajectory |
| j | see eqs. (11), (12), and (13) |

$k_l$     $\dfrac{\left(1 - \sin^2\Lambda\,\cos^2\alpha\right)^{\nu/2}\left\{1 + \cos\left[\arctan\left(\dfrac{\tan \alpha}{\cos \Lambda}\right)\right]\right\}}{2\cos^\nu\Lambda}$ (from appendix E, ref. 6)

$k_w$     $\left(1 + \dfrac{f}{c}\right)^{3/2} - \left(\dfrac{f}{c}\right)^{3/2} - \dfrac{3}{2}\left(\dfrac{f}{c}\right)^{1/2}$ (from appendix E, ref. 6)

| | |
|---|---|
| L | lift |
| m | gross mass of vehicle, slugs |

$P(p)$     $\dfrac{2}{\sqrt{\pi}}\displaystyle\int_0^p e^{-p^2}\,dp$ (This function is tabulated in ref. 8, e.g.)

| | |
|---|---|
| p | distance parameter, $\sqrt{a/2}\,x$ |
| Q | total heat input, Btu |
| q | heat input per square foot, Btu/sq ft |
| $\dot{q}$ | heating rate, Btu/(sq ft)(sec) |
| $\bar{q}$ | dimensionless heating-rate parameter of ref. 2 in nomenclature of this report (see eq. (C1)) |

$\left.\begin{array}{l} q_{0,2} \\ q_{2,4} \\ q_{0,4} \end{array}\right\}$  heat input per sq ft incurred between stations 0 and 2, stations 2 and 4, and stations 0 and 4, respectively

$R_N$  leading-edge radius, ft

$r$  radius of planet, ft

$r_f$  effective constant radius of flight path (see eq. (B3))

$r_{f,i}$  radius of flight path, measured from instantaneous inertial center, ft

$s$  distance measured along flight path from station 2

$V$  flight velocity, ft/sec

$\overline{V}$  ratio of flight velocity to circular velocity, $V/\sqrt{gr}$

$W$  entry vehicle gross weight, lb

$W/A$  wing loading, lb/sq ft

$W_p$  ablated weight, lb

$x,y$  coordinate system with origin at minimum-altitude point of flight path and y-axis passing through center of planet (see fig. 2)

$y_e$  y-coordinate of planet surface

$y_f$  y-coordinate of flight path

$\beta$  exponent in eq. (9) describing variation of atmospheric density with altitude ($\beta^{-1} = 2.35 \times 10^4$ ft for earth (see ref. 2))

$\xi$  distance on entry vehicle from leading-edge stagnation point along streamline (see fig. 7)

$\gamma$  angle of flight path with respect to direction of x-axis

$\Lambda$  geometric sweepback angle

$\Lambda_{ef}$  effective sweepback angle at angle of attack

$\lambda$  leading-edge-radius coordinate angle measured from leading-edge stagnation point (see fig. 7)

$\lambda$      leading-edge-radius coordinate angle measured from leading-edge stagnation point (see fig. 7)

$\nu$      exponent defining variation of leading-edge heating rate with wing sweepback angle

$\rho$      atmospheric density, slugs/cu ft

$\tau$      time, sec

$\varphi$      flight path angle with respect to local horizontal

$\Omega$      vehicle-position angle in instantaneous inertial reference system (see fig. 2), radians

Subscripts:

$f$      final

$H$      horizontal component

$i$      initial

$l$      leading edge of vehicle

$max$      maximum

$ov$      overshoot bound

$s$      spherical stagnation point

$un$      undershoot bound

$w$      windward side of vehicle

$0$      arbitrarily assigned edge of atmosphere for initial entry

$2$      minimum-altitude point of entry phase or atmospheric pass

$4$      arbitrarily assigned edge of atmosphere for exit from atmospheric pass

APPENDIX B


DISCUSSION OF SEVERAL APPROXIMATIONS

The validity of a number of assumptions and approximations made in the present development, regarding error function, flight path angles, and "effective" radius of curvature of the flight path, are discussed herein.


## Error Function

In the discussion of equation (34) it is assumed that the "tail" of the Gaussian error curve contributes little to the area under the complete curve. The Gaussian error curve and the error function are presented in figure 9. The data are taken from the mathematical tables of reference 8 but are presented in the nomenclature of this report and are discussed in relation to the present problem. Figure 9(a) (and also fig. 3) presents the density variation with distance along the flight path encountered by a vehicle during an atmospheric pass of the type considered herein (eqs. (27) and (29)).

Figure 9(b) is a plot of the integral required in equation (30), which is the area under the curve of figure 9(a)

$$P(p) = \frac{2}{\sqrt{\pi}} \int_0^p e^{-p^2}\, dp \tag{B1}$$

where $2/\sqrt{\pi}$ is a normalizing factor. The value of the integral $P(p)$ is insensitive to the value of the upper limit above a value of $p = 1.4$. For $p > 1.4$, $P(p)$ varies only from 0.95 to 1.0.


## Flight-Path Angles

For simplification of equations (1) and (2), it was assumed that $\cos \varphi$ is approximately unity and that $\sin \varphi$ is small compared with the aerodynamic deceleration along the flight path. For small angles, the flight-path angle may be written, from equation (23),

$$\varphi \approx \frac{dh}{dx} = x\left(\frac{1}{r} - \frac{1}{r_f}\right) \tag{B2}$$

From the definitions of  a  and  p, equation (B2) becomes

$$\varphi = \sqrt{\frac{2}{\beta r}} \left( 1 - \frac{1 - 0.85\ G_2\ \dfrac{C_L}{C_R}}{\overline{V}_2^2} \right)^{1/2} p \qquad (B3)$$

For example, for  $G_2 = 10$,  $C_L/C_R = 0.9$  (lift directed away from planet),
$\overline{V}_2 = 1.2$, $p = 1.4$, and  $\beta r = 900$  (earth), the value of  $\varphi$  is $-15^\circ$ and
$\cos\varphi = 0.96$.  Larger values of  $\overline{V}_2$  decrease  $\varphi$.  The approximation
$\cos\varphi = 1$  is, hence, adequate.

For the same example, the component of the aerodynamic force tangent
to the flight path at station 2 is  $G_2 C_D/C_R$  where, from the relation
$C_D/C_R = \sqrt{1 - (C_L/C_R)^2}$, $C_D/C_R = 0.43$.  The component of gravity along
the flight path  $\sin\varphi$  varies from 0 at station 2 where  $\varphi = 0$  to 0.26
at  $p = 1.4$, where  $\varphi = -15^\circ$  or from 0 to 6 percent of the aerodynamic
deceleration at station 2.  Thus, neglecting the term  $\sin\varphi$  in equa-
tion (1) is reasonable.  Also, in preliminary calculations, the perigee
velocity of the vacuum trajectory is often used as the entry velocity.
In this case, the term  $\sin\varphi$  in the equations of motion, in a sense,
has been accounted for in advance.

### Flight Path Radius of Curvature

The present analysis is dependent upon defining a constant "effec-
tive" radius of curvature for the flight path.  The relation used to ob-
tain the numerical results of this report has a form similar to equa-
tion (8) and has been derived by the following reasoning.  First, the
instantaneous radius of curvature for the flight path of a vehicle with
constant aerodynamic coefficients and with the aerodynamic forces large
compared with the force due to gravity (eq. (8) with  $g = 0$) was con-
sidered.  For a specified density at station 2

$$r_{f,i} = \frac{\text{const}}{\rho/\rho_2} \qquad (B4)$$

Note that the minimum radius of curvature occurs at the position of mini-
mum altitude (station 2) and that this relation is independent of the ve-
locity variation along the path.  The radius of curvature at station 2,
hence, was used as a basis for estimating an effective value.  From the

values of figure 9(a), the actual flight path, the solid line of figure 9(c) can be graphically constructed. A constant radius-of-curvature flight path defined by

$$r_f = \frac{r_{f,i,2}}{0.85} \tag{B5}$$

is shown by the dashed line. The two flight paths are in good agreement up to p = 1.4, which encompasses 95 percent of P. For the more general case in which the force due to the gravity field is significant, the constant 0.85 of equation (B5) is applied only to the aerodynamic term of equation (8) to give the empirical relation

$$r_f = \frac{V_2^2}{g - \dfrac{0.85\ C_L \rho_2 V_2^2 A}{2m}} = \frac{\overline{V}_2^2 r}{1 - 0.85\ G_2 \dfrac{C_L}{C_R}} \tag{B6}$$

More accurate techniques for estimating the effective radius of curvature of the flight path will improve the accuracy of the present analysis. The adequacy of the present estimation may be judged by comparison of the results shown in figure 8.

APPENDIX C

COMPARISON WITH REFERENCE 2

This appendix describes how the results of the present analysis can be put in the same form as the results of reference 2, and how such results can be obtained explicitly by using the present analysis. Recall that the sample application given in the text required an iteration procedure. In reference 2, the heating rate to a spherical stagnation point is presented in terms of a dimensionless parameter which, for small path angles and entry at earth, is defined (in terms of the nomenclature of this report) by

$$\bar{\dot{q}}_S = \frac{\dot{q}_S}{590 \sqrt{\dfrac{m}{C_D A R_N}}} \tag{C1}$$

and a dimensionless total heat input per unit area $\bar{q}$ (i.e., $Q/k_2 S$ of eq. (39a), ref. 2) is defined by

$$\bar{q}_S = \frac{q_S}{15,900 \sqrt{\dfrac{m}{C_D A R_N}}} \tag{C2}$$

These dimensionless results can be applied to other planets by using equations (36) and (39a) of reference 2. In this reference, the parameters $\bar{\dot{q}}_S$ and $\bar{q}_S$ are given as functions of the maximum horizontal component of the G load $G_{H,max}$ and the final velocity $\bar{V}_4$ for a given initial velocity $\bar{V}_0$.

The results of the present analysis are given in terms of $\bar{V}_2$ and $G_2$; however, with $\bar{V}_0$ and $\bar{V}_4$ given, $\bar{V}_2$ can be calculated from equations (34) and (35), which gives

$$\frac{\bar{V}_0}{\bar{V}_2} = \sqrt{\frac{\bar{V}_0}{\bar{V}_4}}$$

The solution of equation (36) for $G_2$ using the definitions of $F$ and $a$ is then

$$G_2 = \frac{0.85 \frac{C_L}{C_R} \pm \sqrt{\left(0.85 \frac{C_L}{C_R}\right)^2 - 4E^2\bar{V}_2^2\left(1 - \bar{V}_2^2\right)}}{2E^2\bar{V}_2^2} \tag{C3}$$

where

$$E \equiv \sqrt{\frac{\pi}{2\beta r}} \frac{C_D}{C_R} \frac{1}{\bar{V}_2^2 \ln \frac{\bar{V}_0}{\bar{V}_2}} \tag{C4}$$

and

$$G_{max} = G_2 \left(\frac{G_{max}}{G_2}\right) \tag{C5}$$

At $G_{max}$, the path angle is small, and for small path angles

$$G_{H,max} = G_{max} \frac{C_D}{C_R} \tag{C6a}$$

For the comparison in figure 8(a) the results of reference 2 are presented in terms of $G_{max}$ rather than $G_{H,max}$. In terms of the information given on figure 24 of reference 2, the rearranging and rewriting of equation (C6a) gives

$$G_{max} = G_{H,max} \sqrt{1 + (L/D)^2} \tag{C6b}$$

which is similar to equation (53) of reference 2.

For a three-dimensional stagnation point $\Lambda = \lambda = 0$, reference 10 (pp. 5 through 7) gives the value $\sqrt{2} \ 15.5\times10^{-9}$ for the numerical constant in equation (12). The corresponding value used in reference 2, equation (35), is about 10 percent lower than this value or $19.8\times10^{-9}$. For the purpose of comparison (fig. 8), $19.8\times10^{-9}$ is used. From equations (16) and (C1), with the constant $19.8\times10^{-9}$ instead of $15.5\times10^{-9}$,

the maximum heating-rate parameter is

$$\bar{q} = 0.183 \ \bar{V}_2^2 \ \sqrt{G_2 \frac{C_D}{C_R} \left(\frac{\dot{q}_{max}}{\dot{q}_2}\right)} \tag{C7}$$

Accordingly, from equations (C2), (16), and (47a), and using the definition of a and equations (33) and (37b), the total-heat-input-per-unit-area parameter is

$$\bar{q}_S = \frac{3.09 \ N_{O,4}}{\sqrt{G_2 \frac{C_D}{C_R}}} \ (\bar{V}_O \bar{V}_4)^{3/2} \ \ln \frac{\bar{V}_O}{\bar{V}_4} \tag{C8}$$

The terms in parentheses in equations (C5) and (C7) and $N_{O,4}$ in equation (C8) are given in figures 4 and 6, respectively, where

$$F = \ln \frac{\bar{V}_O}{\bar{V}_2} \tag{C9}$$

APPENDIX D

NUMERICAL VALUES FOR EXAMPLE

The vehicle-design characteristics required in equations (48) and (49) to make the sample calculations presented in table I are those of the vehicle shown in figure 7 and are the same as those used in reference 6. The gross weight $W$ is 10,000 pounds, the fuselage density $\rho_f$ is 20 pounds per cubic foot, the sweep angle $\Lambda$ is $60^\circ$, and the maximum lift-drag ratio is 1. Corresponding to these values, the wing loading $W/A$ is 83 pounds per square foot and $R_N/c = 0.142$.

From figure 2 of reference 6, $(L/D)_{max}$ occurs at an angle of attack $\alpha = 23^\circ$ where $C_L/C_R = C_D/C_R = 0.707$ and $C_R = 0.65$. At $\alpha = 0^\circ$, $C_R = C_D = 0.22$ and $C_L = 0$.

The term $\nu$, which gives the effect of wing sweep on heating, is taken as 1.5. The $k$ terms required in equations (48) and (49) have the following numerical values: $k_l = 1.0$ at $\alpha = 0^\circ$ and 1.17 at $\alpha = 23^\circ$, $k_w = 0.5$ at $\alpha = 23^\circ$.

APPENDIX E

CALCULATION OF CORRIDOR DEPTH

The corridor depth $d$ is defined as the difference in the perigees, of the vacuum trajectories of the overshoot and undershoot bounds:

$$d = h_{p,ov} - h_{p,un} \tag{E1}$$

For a constant angle-of-attack entry on the undershoot bound, equation (28) of reference 7 gives the following relation for the vacuum perigee altitude in feet where $\varphi_2 = 0$; $C_{R,un} = C_{R,2} = C_{R,1}$; $G_{un} = G_{max}$; $(C_L/C_R)_{un} = (C_L/C_R)_1$; and $V_0 = V$:

$$\frac{h_{p,un}}{r} = -\frac{1}{\beta r}\left[\ln \frac{2G_{un}W}{C_{R,un}\rho_{h=0}V_0^2 A} + \frac{G_{un}\left(\frac{C_L}{C_R}\right)_{un}}{\overline{V}_0^2 - 1}\right] \tag{E2}$$

In the present examples, a perigee altitude defined by the G load with zero lift assumed during the entry phase is used for the overshoot bound. From equation (14) for $G$, and equation (9) for the density variation with altitude,

$$\frac{h_{p,ov}}{r} = -\frac{1}{\beta r}\ln \frac{2G_{ov}W}{C_{R,ov}\rho_{h=0}V_0^2 A} \tag{E3}$$

Substituting equations (E2) and (E3) in (E1) gives the equation for corridor depth

$$d = \frac{1}{\beta}\left[\ln \frac{G_{un}C_{R,ov}}{G_{ov}C_{R,un}} + \frac{G_{un}\left(\frac{C_L}{C_R}\right)_{un}}{\overline{V}_0^2 - 1}\right] \tag{E4}$$
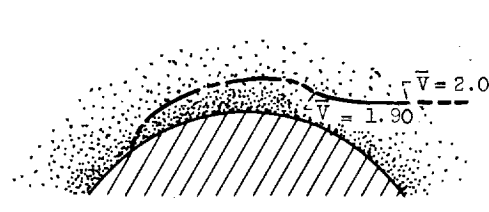
The numerical values used are given in appendix D or in the discussion of table I. Equation (E4) gives either the corridor depth or the altitude of the tangent entry path above the undershoot bound depending on the value of $G_{ov}$ used.

34

REFERENCES
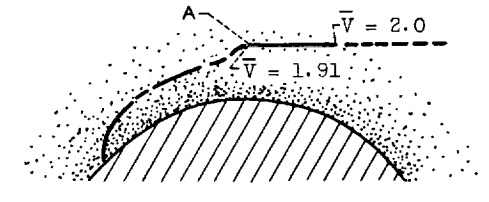
1. Himmel, S. C., Dugan, J. F., Jr., Luidens, R. W., and Weber, R. J.:
   A Study of Manned Nuclear-Rocket Missions to Mars. Paper 61-49,
   Inst. Aerospace Sci., Inc., 1961.

2. Chapman, Dean R.: An Approximate Analytical Method for Studying
   Entry into Planetary Atmospheres. NACA TR R-11, 1959. (Supersedes
   NACA TN 4276.)

3. Chapman, Dean R.: An Analysis of the Corridor and Guidance Require-
   ments for Supercircular Entry into Planetary Atmospheres. NASA
   TR R-55, 1959.

4. Levy, Lionel L., Jr.: An Approximate Analytical Method for Studying
   Atmosphere Entry of Vehicles with Modulated Aerodynamic Forces.
   NASA TN D-319, 1960.

5. Levy, Lionel L., Jr.: The Use of Drag Modulation to Limit the Rate
   at Which Deceleration Increases During Nonlifting Entry. NASA TN
   D-1037, 1961.

6. Luidens, Roger W.: Flight-Path Characteristics for Decelerating
   from Supercircular Speed. NASA TN D-1091, 1961.

7. Luidens, Roger W.: Approximate Analysis of Atmospheric Entry Cor-
   ridors and Angles. NASA TN D-590, 1961.

8. Federal Works Agency: Tables of Probability Functions. Vol. 1.
   NBS, 1941.

9. Grant, Frederick C.: Simple Formulas for Stagnation-Point Convective
   Heat Loads in Lunar Return. NASA TN D-890, 1961.

10. Lees, Lester: Space Technology. Lecture 6A, Eng. Extension, Univ.
    Calif., 1958.

TABLE I. - HEAT INPUT ON FLIGHT PATHS ENTERING AT TWICE CIRCULAR AND DECELERATING

TO ZERO VELOCITY, $G_{max}$, 10; $(L/D)_{max}$, 1.0
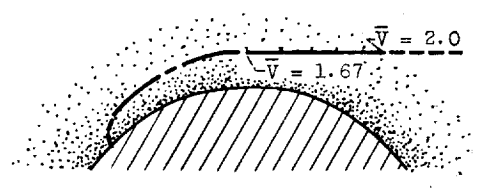
(a) Undershoot bound

| Flight path (a) | Flight phase | Ratio of heat input to vehicle gross weight, Q/W, Btu/lb | | | Altitude above under-shoot bound, miles (b) |
| --- | --- | --- | --- | --- | --- |
| | | Leading edge | Windward side | Total | |
|  | Entry[c] | 66 | 53 | | |
| | Deceleration | 289 | 44 | | 0 |
| | Total | 355 | [d]97 | 452 | |

(b) Overshoot bound

| | Entry[c] | 102 | ~0 | | |
| --- | --- | --- | --- | --- | --- |
|  | Deceleration | 293 | 46 | | 10.5 |
| | Total | [d]395 | 46 | 441 | |

(c) Tangent entry

| | Entry[c] | 194 | ~0 | | |
| --- | --- | --- | --- | --- | --- |
|  | Deceleration | 196 | 23 | | 5.7 |
| | Total | 390 | 23 | 413 | |

[a] ———— Entry (present analysis).
———·—— Deceleration (ref. 6).

[b]Appendix E.

[c]Present analysis.

[d]Values combined for design total, 492.

36



(a) Atmospheric pass with positive lift.

(b) Atmospheric pass with zero lift.

(c) Atmospheric pass with negative lift.

(d) Phases of atmospheric-braking path.

(e) Aerodynamic entry corridor.
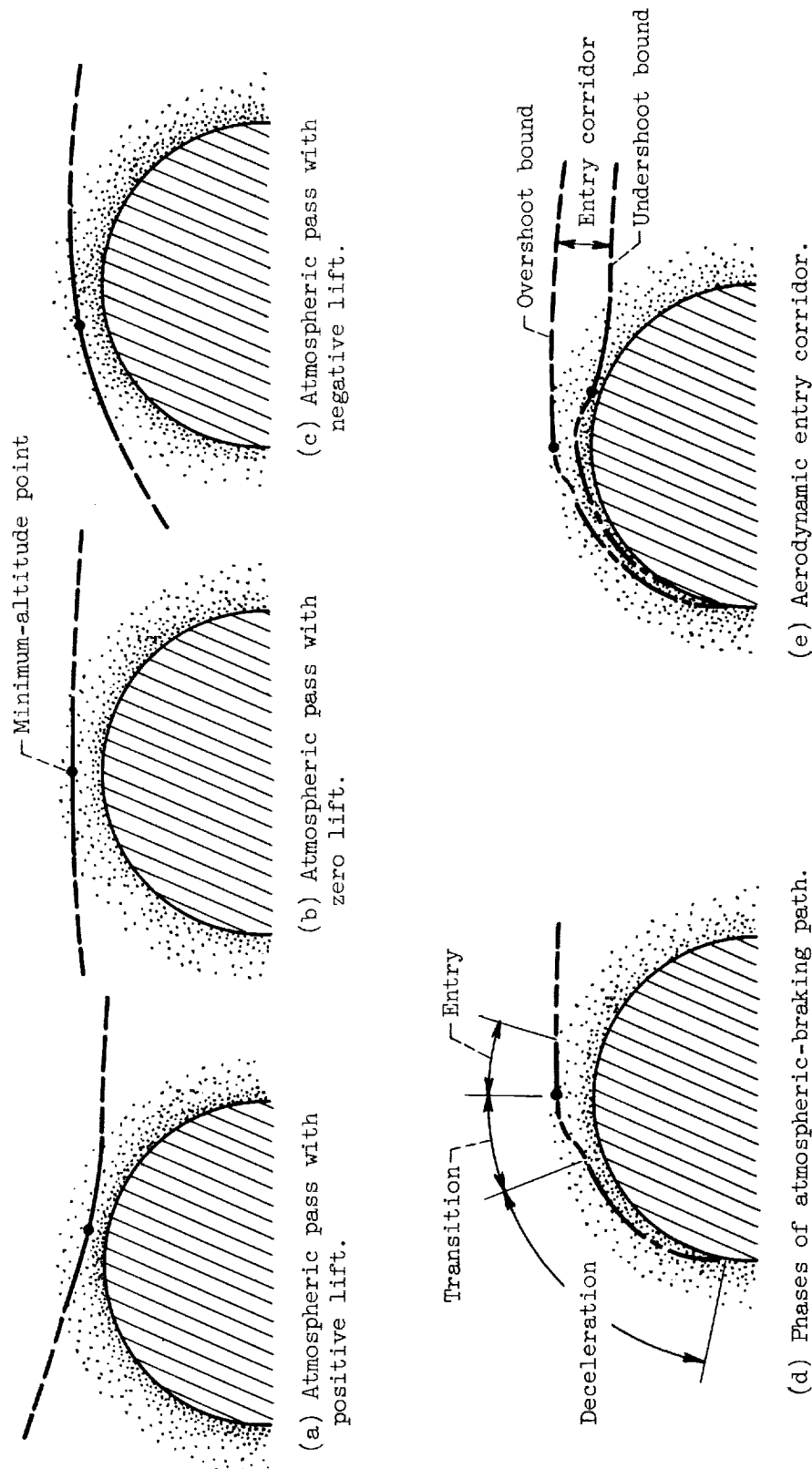
Figure 1. - Typical flight paths encountering significant atmospheric forces. Present analysis applies to portion of flight path denoted by a solid line.

Figure 2. - Flight-path coordinate systems and nomenclature.
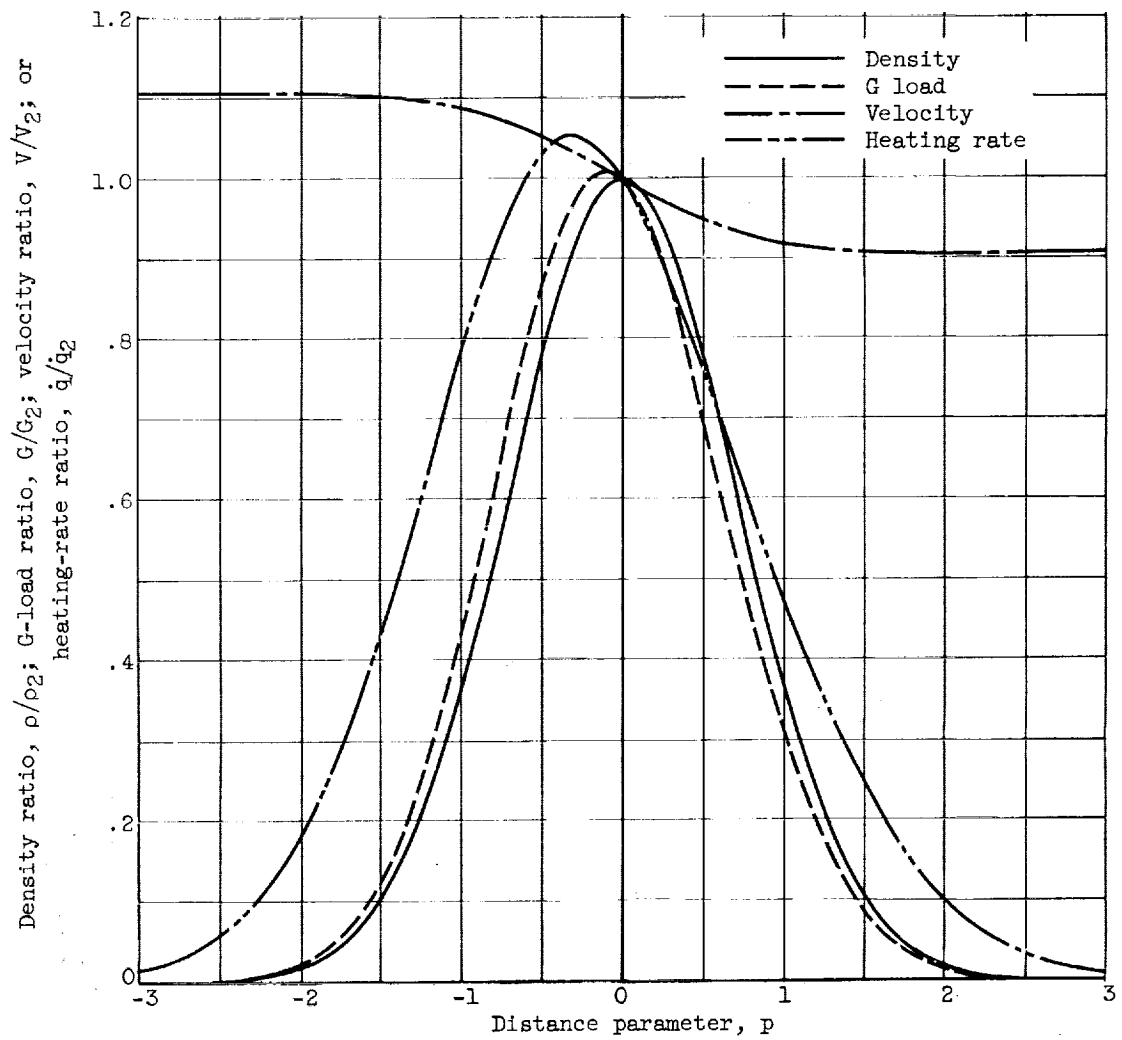
(a) Flight path parameter  F, 0.1.

Figure 3. - Variation of density ratio, G-load ratio, velocity ratio, and heating-rate ratio with distance along flight path.
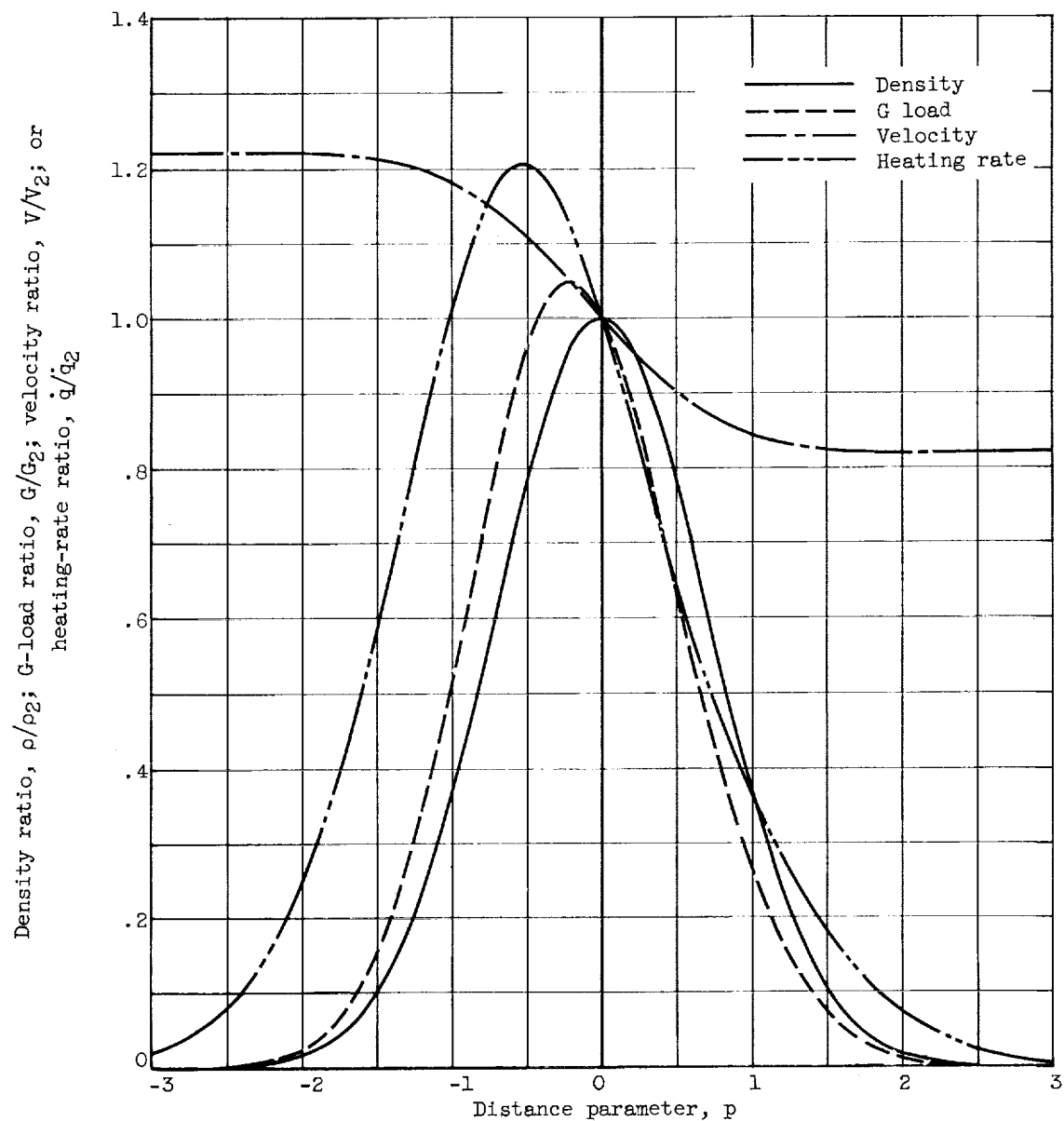
(b) Flight-path parameter  F, 0.2.

Figure 3. - Continued.  Variation of density ratio, G-load ratio, ve-
locity ratio, and heating-rate ratio with distance along flight path.
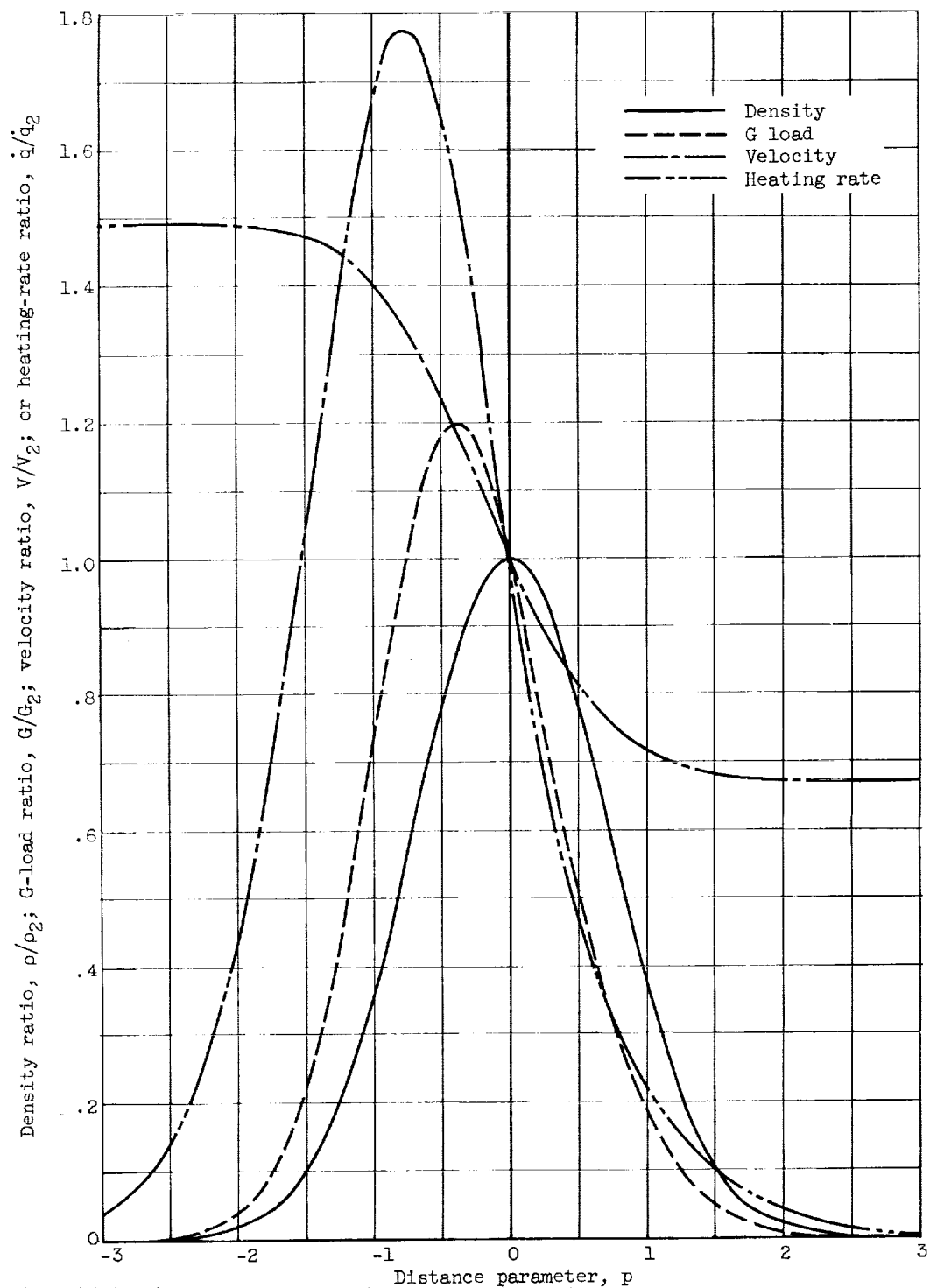
(c) Flight-path parameter F, 0.4.

Figure 3. - Concluded. Variation of density ratio, G-load ratio, velocity ratio, and heating-rate ratio with distance along flight path.
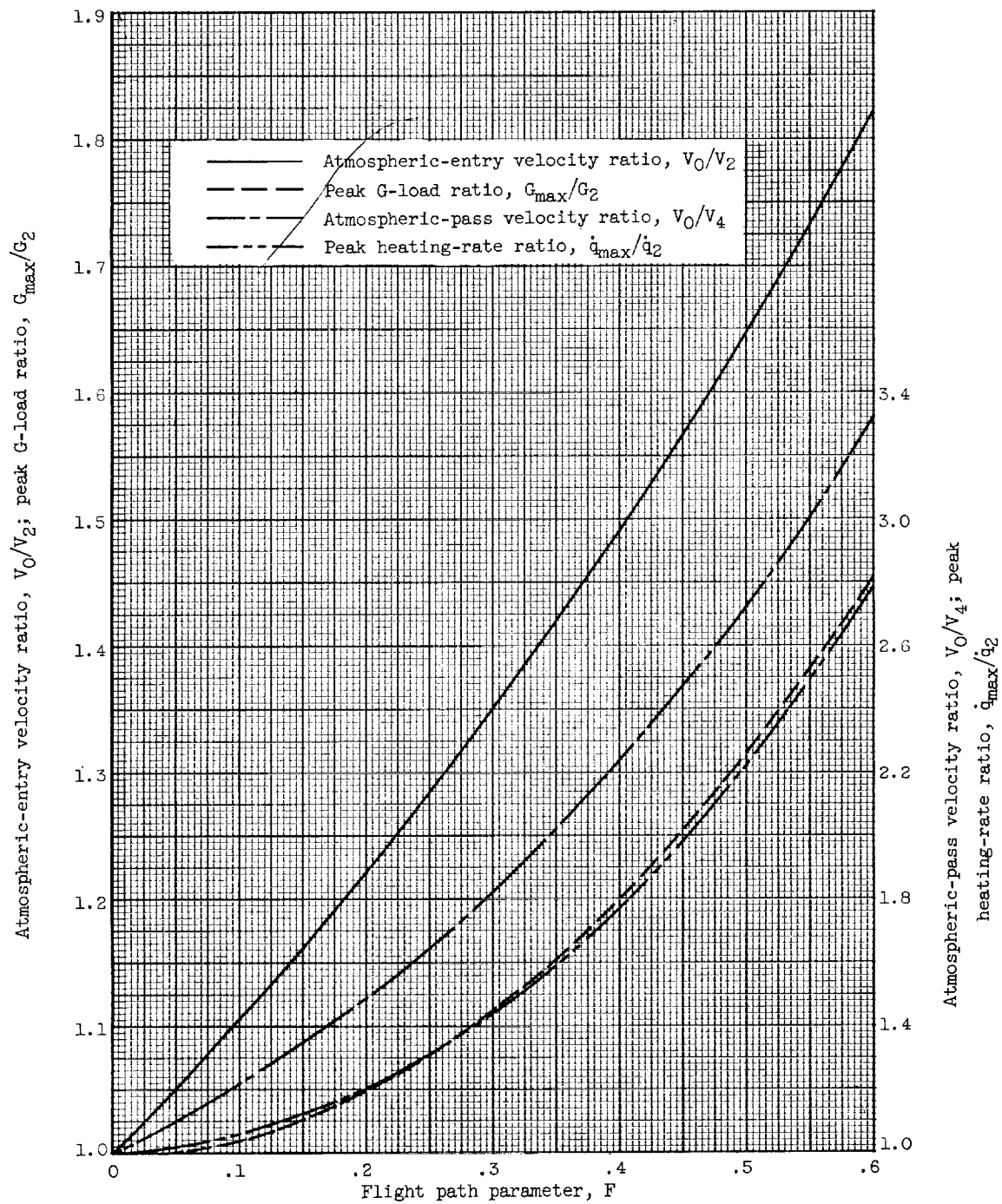
Figure 4. - Variation of atmospheric-entry velocity ratio, atmospheric-
pass velocity ratio, peak G-load ratio, and peak heating-rate ratio
with flight-path parameter.
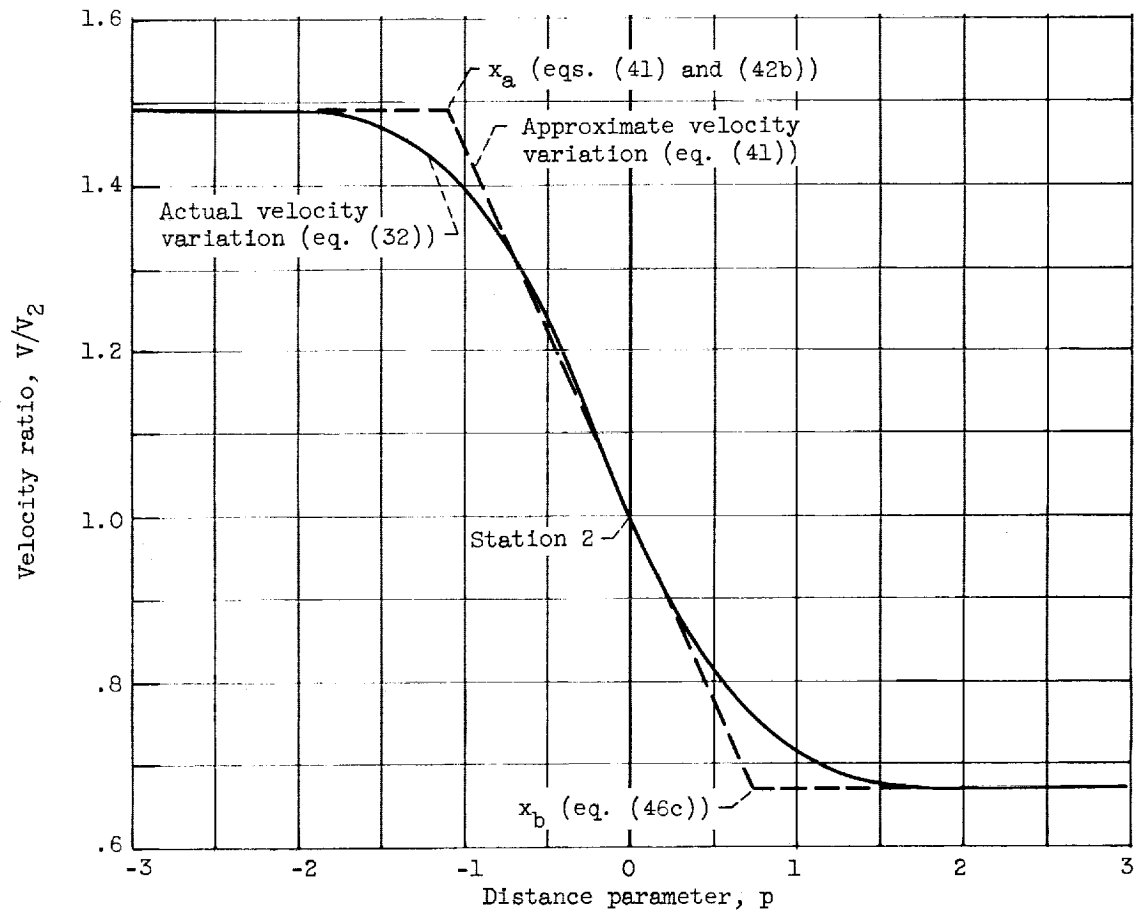
Figure 5. - Comparison of velocity variation with distance assumed for heat input analysis and actual velocity variation. Flight-path parameter, F, 0.4.
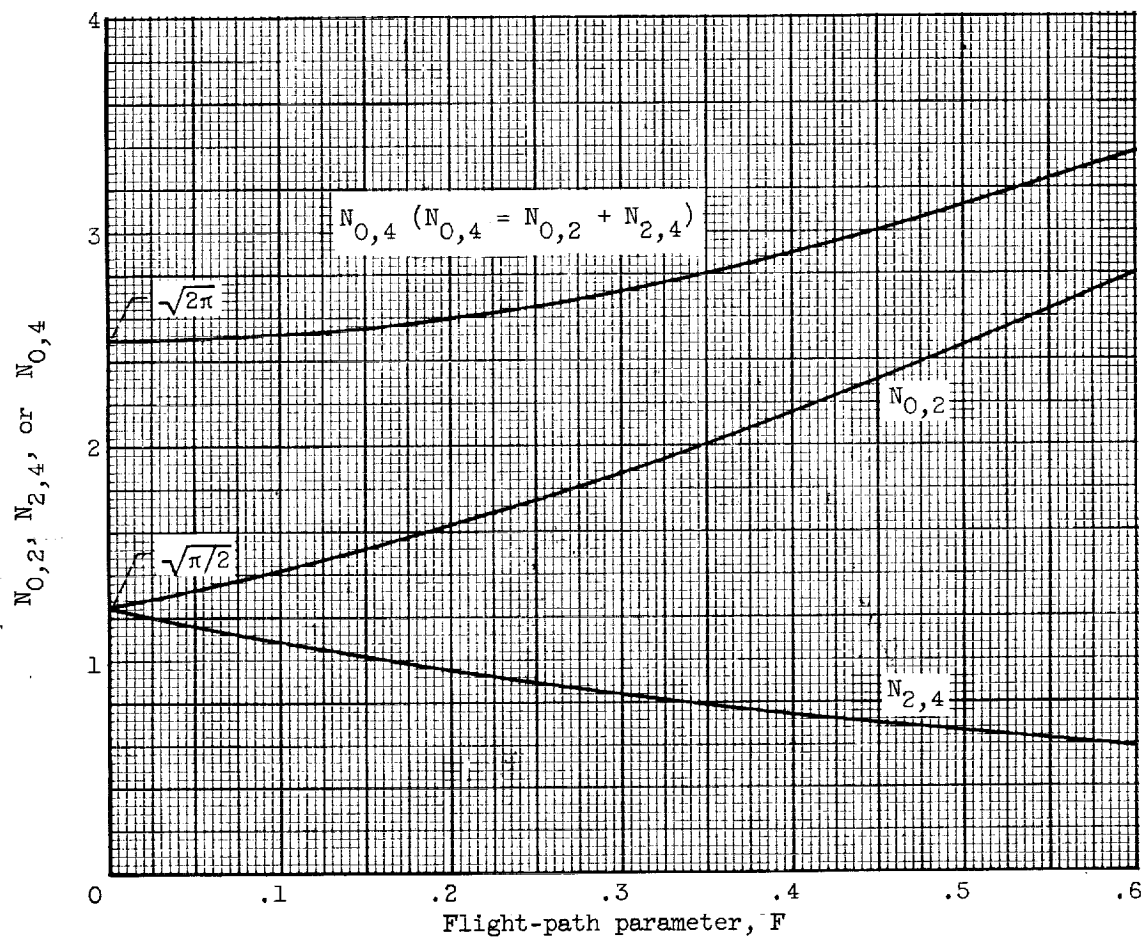
Figure 6. - Variation of $N_{0,2}$, $N_{2,4}$, and $N_{0,4}$ with flight-path parameter.

Plan view

Section A-A

Section B-B
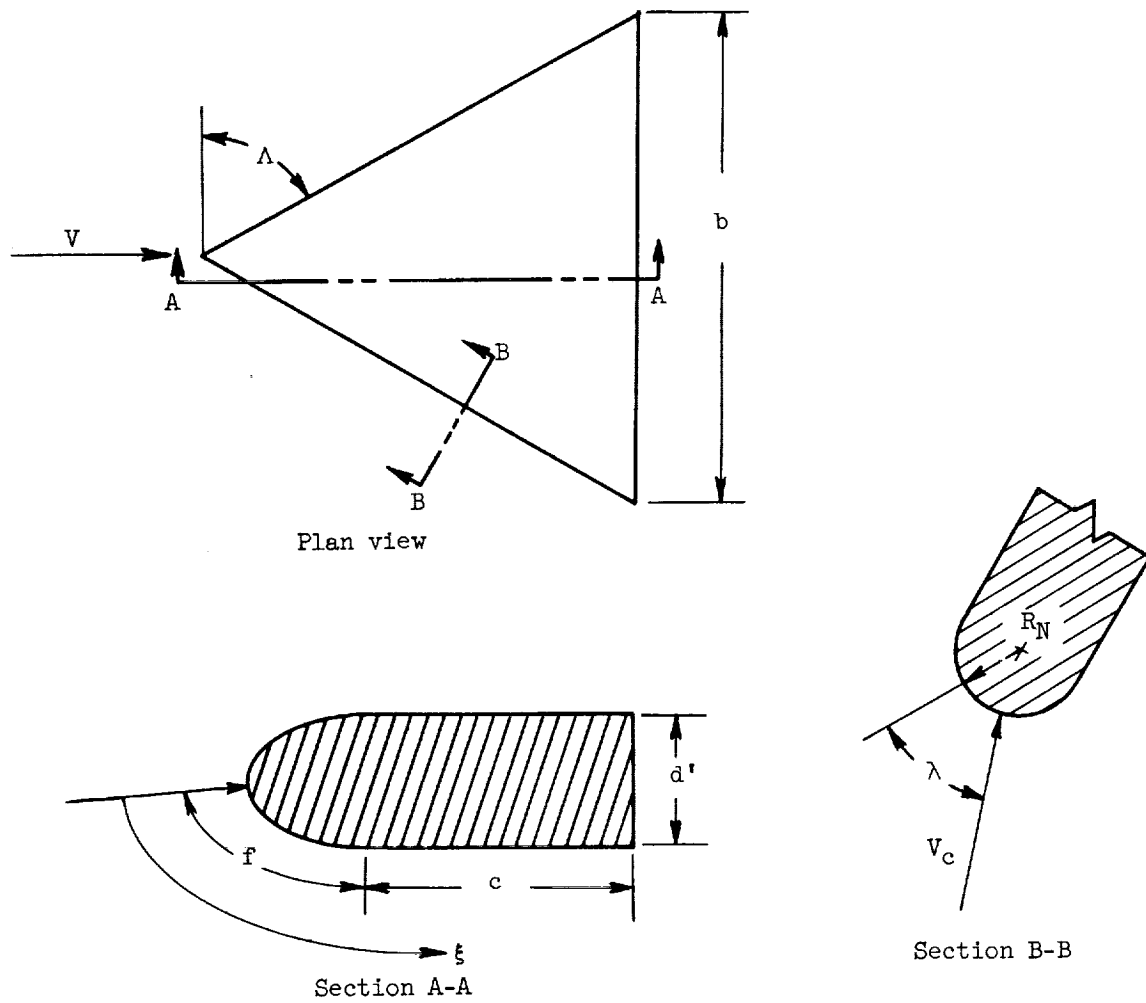
Figure 7. - Vehicle geometry and nomenclature.
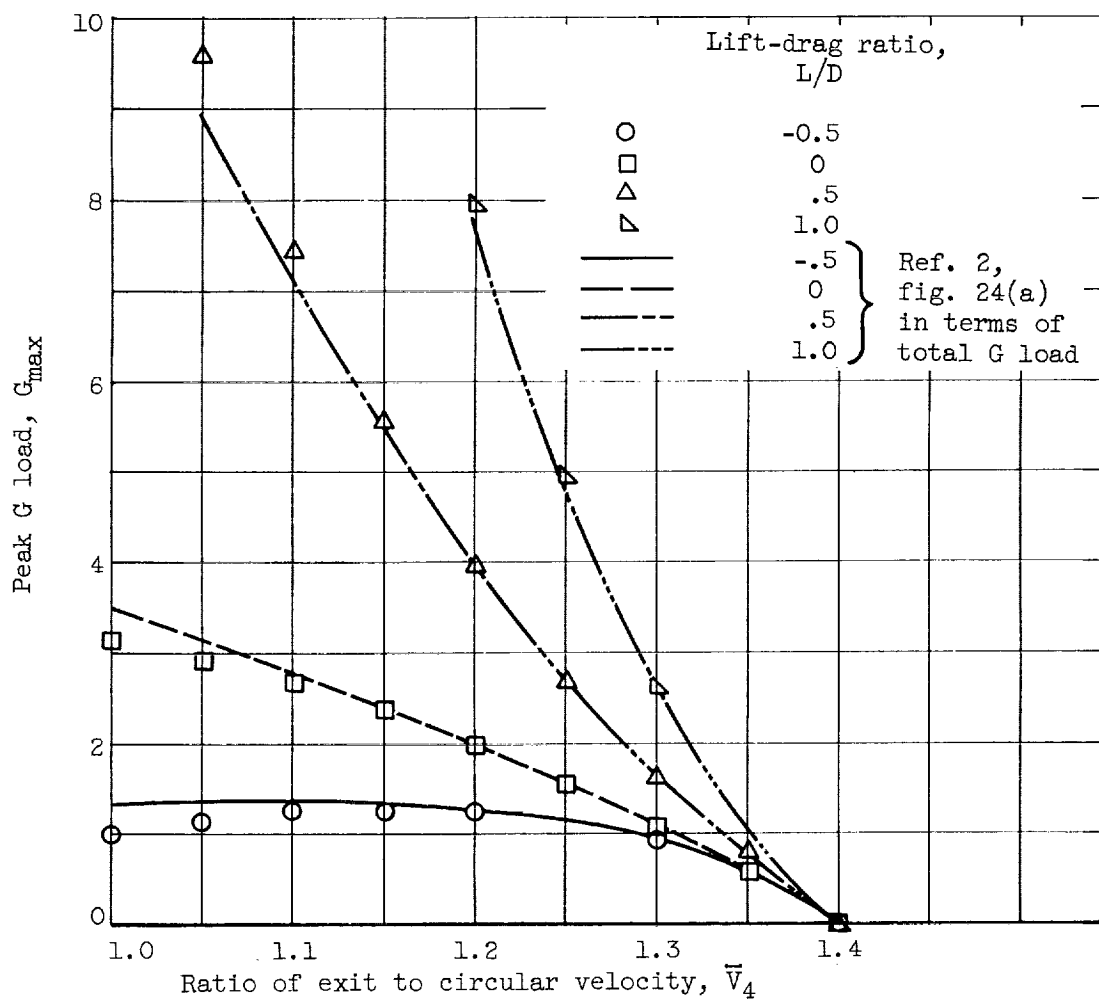
(a) Peak G load.

Figure 8. - Comparison of results of present analysis for atmospheric pass with results of reference 2. Ratio of flight to circular velocity at entry, 1.40.
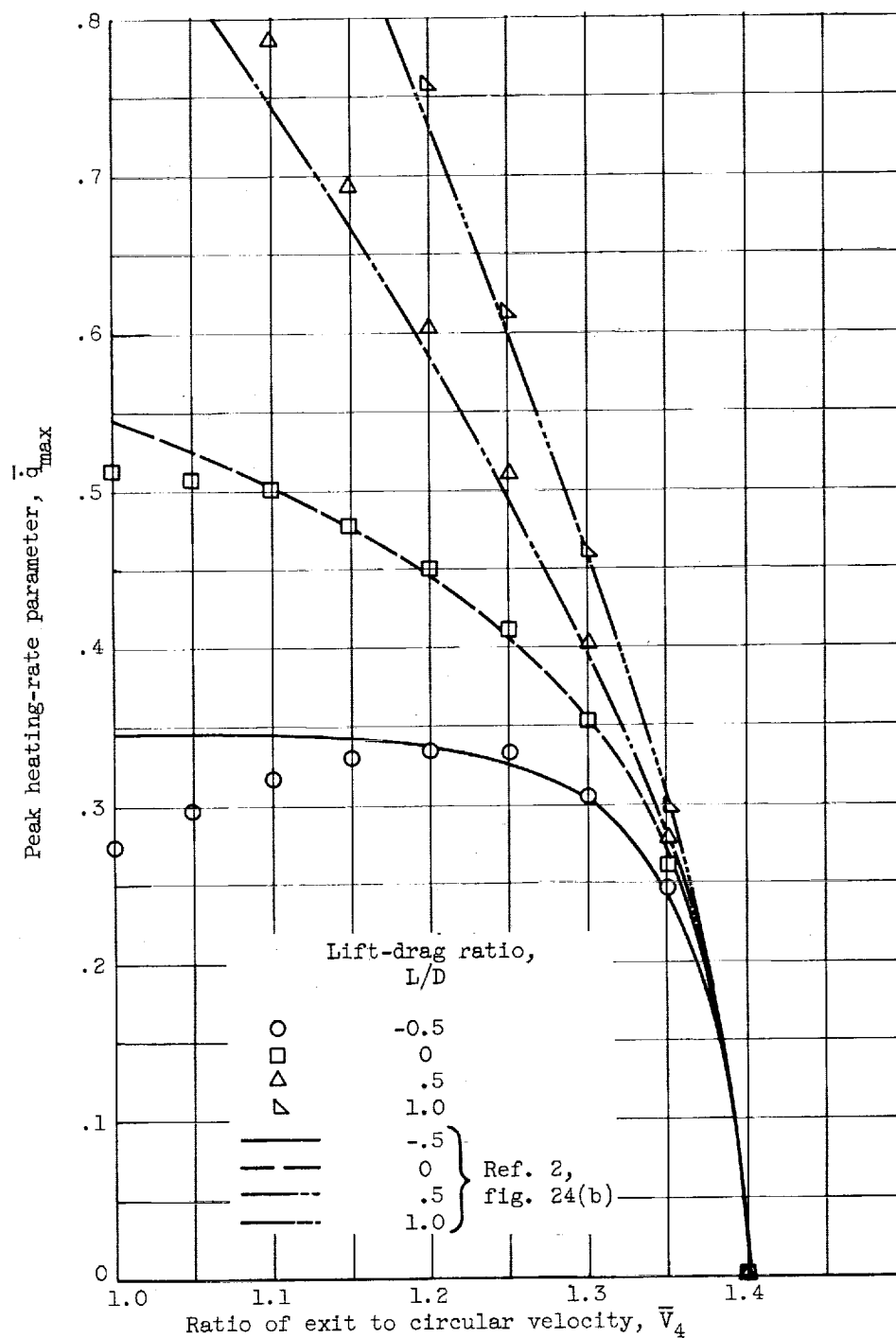
(b) Peak heating rate.

Figure 8. - Continued. Comparison of results of present
analysis for atmospheric pass with results of reference 2.
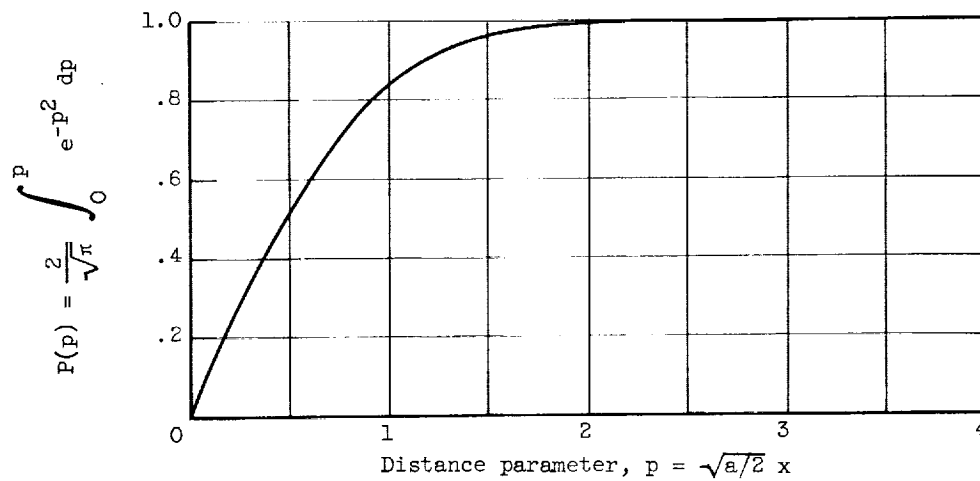Ratio of flight to circular velocity at entry, 1.40.
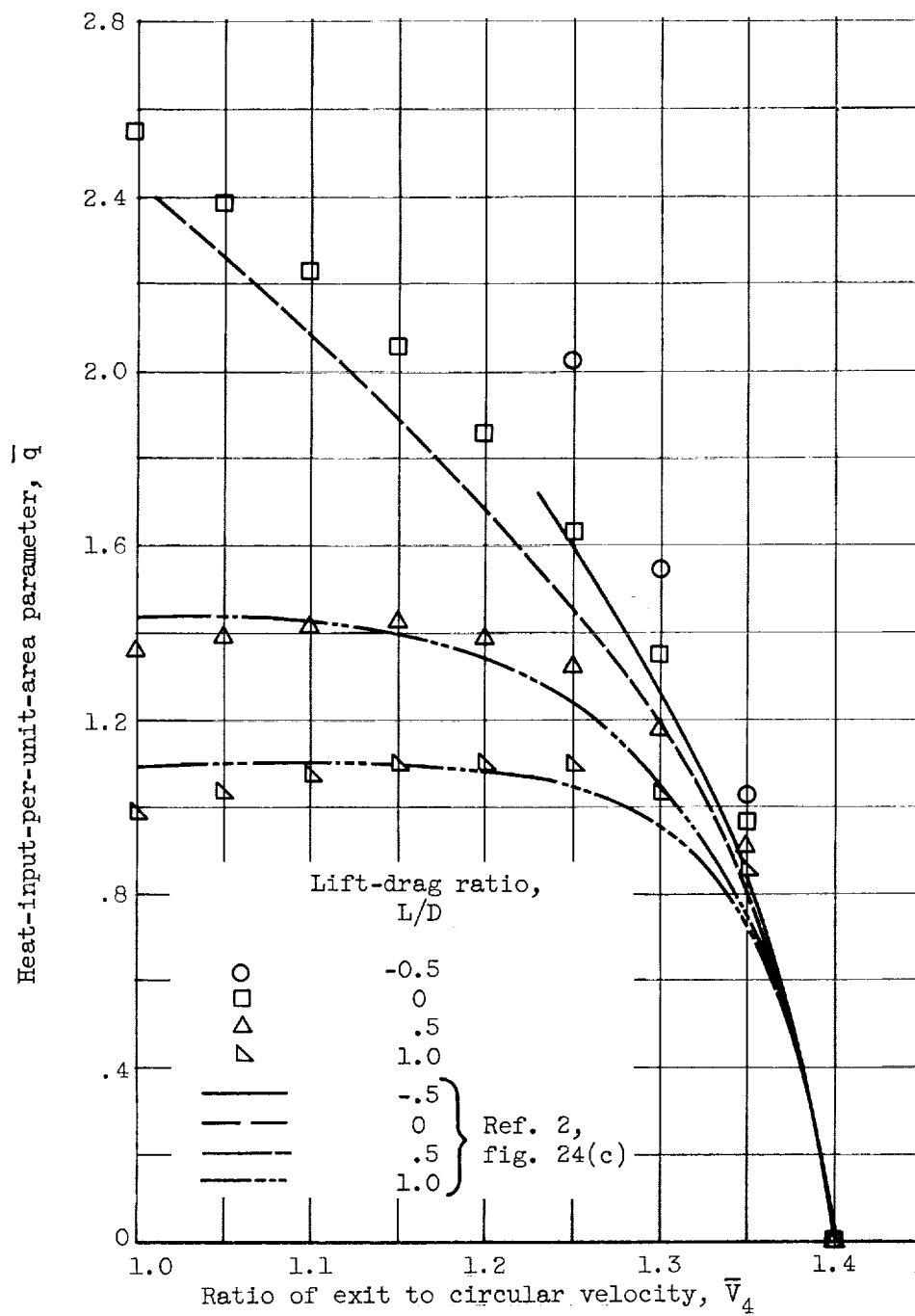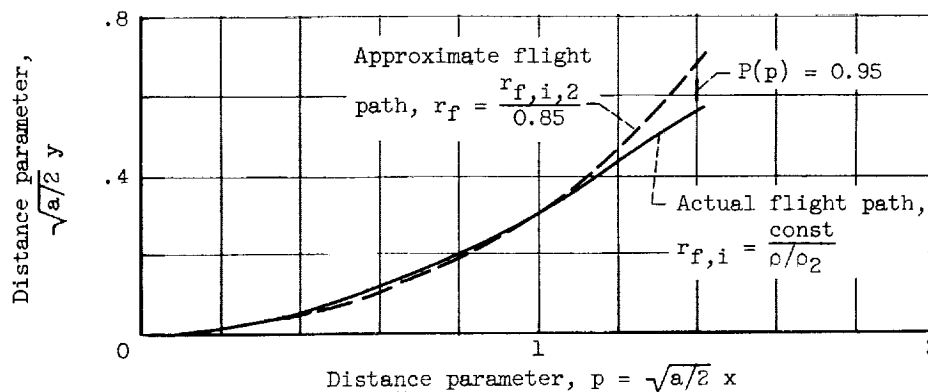
(c) Heat input per unit area.

Figure 8. - Concluded. Comparison of results of present analysis for atmospheric pass with results of reference 2. Ratio of flight to circular velocity at entry, 1.40.

Density ratio, $\rho/\rho_2 = e^{-p^2}$
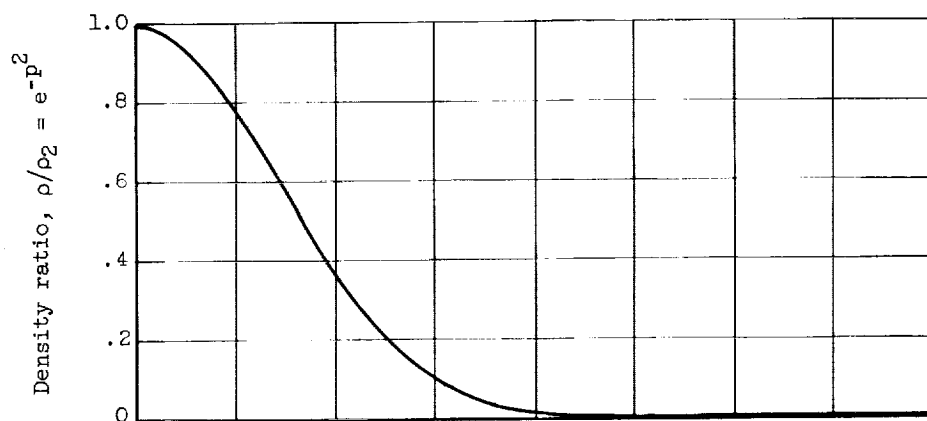
(a) Density variation along flight path during an atmospheric entry.



$P(p) = \dfrac{2}{\sqrt{\pi}} \displaystyle\int_0^p e^{-p^2}\, dp$

Distance parameter, $p = \sqrt{a/2}\; x$

(b) Representation of integral in equation (30).



Distance parameter, $\sqrt{a/2}\; y$

Approximate flight path, $r_f = \dfrac{r_{f,i,2}}{0.85}$

$P(p) = 0.95$

Actual flight path, $r_{f,i} = \dfrac{const}{\rho/\rho_2}$

Distance parameter, $p = \sqrt{a/2}\; x$

(c) Approximation to the flight path.

Figure 9. - Error function and flight-path radius of curvature.

NASA TN D-1280
National Aeronautics and Space Administration.
APPROXIMATE ANALYSIS OF G LOADS AND HEATING DURING ATMOSPHERIC ENTRIES AND PASSES WITH CONSTANT AERODYNAMIC COEFFICIENTS.
Roger W. Luidens. July 1962. 48p. OTS price,
$1.25. . (NASA TECHNICAL NOTE D-1280)

Approximate closed-form solutions are derived for the variation of atmospheric density, G load, and heating rate with distance along the flight path and for peak values of G load and heating rate. The total heat input is given as a function of the velocity decrease and G load. The solutions are applicable to atmospheric entries or passes of lifting or nonlifting vehicles with constant aerodynamic coefficients when the curvature of the flight path is less than the curvature of the planet surface.

NASA TN D-1280
National Aeronautics and Space Administration.
APPROXIMATE ANALYSIS OF G LOADS AND HEATING DURING ATMOSPHERIC ENTRIES AND PASSES WITH CONSTANT AERODYNAMIC COEFFICIENTS.
Roger W. Luidens. July 1962. 48p. OTS price,
$1.25. . (NASA TECHNICAL NOTE D-1280)

Approximate closed-form solutions are derived for the variation of atmospheric density, G load, and heating rate with distance along the flight path and for peak values of G load and heating rate. The total heat input is given as a function of the velocity decrease and G load. The solutions are applicable to atmospheric entries or passes of lifting or nonlifting vehicles with constant aerodynamic coefficients when the curvature of the flight path is less than the curvature of the planet surface.

NASA TN D-1280
National Aeronautics and Space Administration.
APPROXIMATE ANALYSIS OF G LOADS AND HEATING DURING ATMOSPHERIC ENTRIES AND PASSES WITH CONSTANT AERODYNAMIC COEFFICIENTS.
Roger W. Luidens. July 1962. 48p. OTS price,
$1.25. . (NASA TECHNICAL NOTE D-1280)

Approximate closed-form solutions are derived for the variation of atmospheric density, G load, and heating rate with distance along the flight path and for peak values of G load and heating rate. The total heat input is given as a function of the velocity decrease and G load. The solutions are applicable to atmospheric entries or passes of lifting or nonlifting vehicles with constant aerodynamic coefficients when the curvature of the flight path is less than the curvature of the planet surface.

NASA TN D-1280
National Aeronautics and Space Administration.
APPROXIMATE ANALYSIS OF G LOADS AND HEATING DURING ATMOSPHERIC ENTRIES AND PASSES WITH CONSTANT AERODYNAMIC COEFFICIENTS.
Roger W. Luidens. July 1962. 48p. OTS price,
$1.25. . (NASA TECHNICAL NOTE D-1280)

Approximate closed-form solutions are derived for the variation of atmospheric density, G load, and heating rate with distance along the flight path and for peak values of G load and heating rate. The total heat input is given as a function of the velocity decrease and G load. The solutions are applicable to atmospheric entries or passes of lifting or nonlifting vehicles with constant aerodynamic coefficients when the curvature of the flight path is less than the curvature of the planet surface.